# Study of $\bar{B} \to X_u \ell \bar{\nu}$ decays in $B\bar{B}$ events tagged by a fully reconstructed $B$-meson decay and determination of $|V_{ub}|$

J. P. Lees,[1] V. Poireau,[1] V. Tisserand,[1] J. Garra Tico,[2] E. Grauges,[2] M. Martinelli,[3a,3b] D. A. Milanes,[3a] A. Palano,[3a,3b] M. Pappagallo,[3a,3b] G. Eigen,[4] B. Stugu,[4] D. N. Brown,[5] L. T. Kerth,[5] Yu. G. Kolomensky,[5] G. Lynch,[5] K. Tackmann,[5] H. Koch,[6] T. Schroeder,[6] D. J. Asgeirsson,[7] C. Hearty,[7] T. S. Mattison,[7] J. A. McKenna,[7] A. Khan,[8] V. E. Blinov,[9] A. R. Buzykaev,[9] V. P. Druzhinin,[9] V. B. Golubev,[9] E. A. Kravchenko,[9] A. P. Onuchin,[9] S. I. Serednyakov,[9] Yu. I. Skovpen,[9] E. P. Solodov,[9] K. Yu. Todyshev,[9] A. N. Yushkov,[9] M. Bondioli,[10] D. Kirkby,[10] A. J. Lankford,[10] M. Mandelkern,[10] D. P. Stoker,[10] H. Atmacan,[11] J. W. Gary,[11] F. Liu,[11] O. Long,[11] G. M. Vitug,[11] C. Campagnari,[12] T. M. Hong,[12] D. Kovalskyi,[12] J. D. Richman,[12] C. A. West,[12] A. M. Eisner,[13] J. Kroseberg,[13] W. S. Lockman,[13] A. J. Martinez,[13] T. Schalk,[13] B. A. Schumm,[13] A. Seiden,[13] C. H. Cheng,[14] D. A. Doll,[14] B. Echenard,[14] K. T. Flood,[14] D. G. Hitlin,[14] P. Ongmongkolkul,[14] F. C. Porter,[14] A. Y. Rakitin,[14] R. Andreassen,[15] M. S. Dubrovin,[15] Z. Huard,[15] B. T. Meadows,[15] M. D. Sokoloff,[15] L. Sun,[15] P. C. Bloom,[16] W. T. Ford,[16] A. Gaz,[16] M. Nagel,[16] U. Nauenberg,[16] J. G. Smith,[16] S. R. Wagner,[16] R. Ayad,[17,*] W. H. Toki,[17] B. Spaan,[18] M. J. Kobel,[19] K. R. Schubert,[19] R. Schwierz,[19] D. Bernard,[20] M. Verderi,[20] P. J. Clark,[21] S. Playfer,[21] D. Bettoni,[22a] C. Bozzi,[22a] R. Calabrese,[22a,22b] G. Cibinetto,[22a,22b] E. Fioravanti,[22a,22b] I. Garzia,[22a,22b] E. Luppi,[23] M. Munerato,[22a,22b] M. Negrini,[22a,22b] A. Petrella,[22a,22b] L. Piemontese,[22a] V. Santoro,[22a,22b] R. Baldini-Ferroli,[23] A. Calcaterra,[23] R. de Sangro,[23] G. Finocchiaro,[23] M. Nicolaci,[23] P. Patteri,[23] I. M. Peruzzi,[23,†] M. Piccolo,[23] M. Rama,[23] A. Zallo,[23] R. Contri,[24a,24b] E. Guido,[24a,24b] M. Lo Vetere,[24a,24b] M. R. Monge,[24a,24b] S. Passaggio,[24a] C. Patrignani,[24a,24b] E. Robutti,[24a] B. Bhuyan,[25] V. Prasad,[25] C. L. Lee,[26] M. Morii,[26] A. J. Edwards,[27] A. Adametz,[28] J. Marks,[28] U. Uwer,[28] F. U. Bernlochner,[29] M. Ebert,[29] H. M. Lacker,[29] T. Lueck,[29] P. D. Dauncey,[30] M. Tibbetts,[30] P. K. Behera,[31] U. Mallik,[31] C. Chen,[32] J. Cochran,[32] W. T. Meyer,[32] S. Prell,[32] E. I. Rosenberg,[32] A. E. Rubin,[32] A. V. Gritsan,[33] Z. J. Guo,[33] N. Arnaud,[34] M. Davier,[34] G. Grosdidier,[34] F. Le Diberder,[34] A. M. Lutz,[34] B. Malaescu,[34] P. Roudeau,[34] M. H. Schune,[34] A. Stocchi,[34] G. Wormser,[34] D. J. Lange,[35] D. M. Wright,[35] I. Bingham,[36] C. A. Chavez,[36] J. P. Coleman,[36] J. R. Fry,[36] E. Gabathuler,[36] D. E. Hutchcroft,[36] D. J. Payne,[36] C. Touramanis,[36] A. J. Bevan,[37] F. Di Lodovico,[37] R. Sacco,[37] M. Sigamani,[37] G. Cowan,[38] D. N. Brown,[39] C. L. Davis,[39] A. G. Denig,[40] M. Fritsch,[40] W. Gradl,[40] A. Hafner,[40] E. Prencipe,[40] K. E. Alwyn,[41] D. Bailey,[41] R. J. Barlow,[41,‡] G. Jackson,[41] G. D. Lafferty,[41] R. Cenci,[42] B. Hamilton,[42] A. Jawahery,[42] D. A. Roberts,[42] G. Simi,[42] C. Dallapiccola,[43] R. Cowan,[44] D. Dujmic,[44] G. Sciolla,[44] D. Lindemann,[45] P. M. Patel,[45] S. H. Robertson,[45] M. Schram,[45] P. Biassoni,[46a,46b] A. Lazzaro,[46a,46b] V. Lombardo,[46a] N. Neri,[46a,46b] F. Palombo,[46a,46b] S. Stracka,[46a,46b] L. Cremaldi,[47] R. Godang,[47,§] R. Kroeger,[47] P. Sonnek,[47] D. J. Summers,[47] X. Nguyen,[48] P. Taras,[48] G. De Nardo,[49a,49b] D. Monorchio,[49a,49b] G. Onorato,[49a,49b] C. Sciacca,[49a,49b] G. Raven,[50] H. L. Snoek,[50] C. P. Jessop,[51] K. J. Knoepfel,[51] J. M. LoSecco,[51] W. F. Wang,[51] K. Honscheid,[52] R. Kass,[52] J. Brau,[53] R. Frey,[53] N. B. Sinev,[53] D. Strom,[53] E. Torrence,[53] E. Feltresi,[54a,54b] N. Gagliardi,[54a,54b] M. Margoni,[54a,54b] M. Morandin,[54a] M. Posocco,[54a] M. Rotondo,[54a] F. Simonetto,[54a,54b] R. Stroili,[54a,54b] E. Ben-Haim,[55] M. Bomben,[55] G. R. Bonneaud,[55] H. Briand,[55] G. Calderini,[55] J. Chauveau,[55] O. Hamon,[55] Ph. Leruste,[55] G. Marchiori,[55] J. Ocariz,[55] S. Sitt,[55] M. Biasini,[56a,56b] E. Manoni,[56a,56b] S. Pacetti,[56a,56b] A. Rossi,[56a,56b] C. Angelini,[57a,57b] G. Batignani,[57a,57b] S. Bettarini,[57a,57b] M. Carpinelli,[57a,57b,‖] G. Casarosa,[57a,57b] A. Cervelli,[57a,57b] F. Forti,[57a,57b] M. A. Giorgi,[57a,57b] A. Lusiani,[57a,57c] B. Oberhof,[57a,57b] E. Paoloni,[57a,57b] A. Perez,[57a] G. Rizzo,[57a,57b] J. J. Walsh,[57a] D. Lopes Pegna,[58] C. Lu,[58] J. Olsen,[58] A. J. S. Smith,[58] A. V. Telnov,[58] F. Anulli,[59a] G. Cavoto,[59a] R. Faccini,[59a,59b] F. Ferrarotto,[59a] F. Ferroni,[59a,59b] M. Gaspero,[59a,59b] L. Li Gioi,[59a] M. A. Mazzoni,[59a] G. Piredda,[59a] C. Bünger,[60] O. Grünberg,[60] T. Hartmann,[60] T. Leddig,[60] H. Schröder,[60] R. Waldi,[60] T. Adye,[61] E. O. Olaiya,[61] F. F. Wilson,[61] S. Emery,[62] G. Hamel de Monchenault,[62] G. Vasseur,[62] Ch. Yèche,[62] D. Aston,[63] D. J. Bard,[63] R. Bartoldus,[63] C. Cartaro,[63] M. R. Convery,[63] J. Dorfan,[63] G. P. Dubois-Felsmann,[63] W. Dunwoodie,[63] R. C. Field,[63] M. Franco Sevilla,[63] B. G. Fulsom,[63] A. M. Gabareen,[63] M. T. Graham,[63] P. Grenier,[63] C. Hast,[63] W. R. Innes,[63] M. H. Kelsey,[63] H. Kim,[63] P. Kim,[63] M. L. Kocian,[63] D. W. G. S. Leith,[63] P. Lewis,[63] S. Li,[63] B. Lindquist,[63] S. Luitz,[63] V. Luth,[63] H. L. Lynch,[63] D. B. MacFarlane,[63] D. R. Muller,[63] H. Neal,[63] S. Nelson,[63] I. Ofte,[63] M. Perl,[63] T. Pulliam,[63] B. N. Ratcliff,[63] A. Roodman,[63] A. A. Salnikov,[63] R. H. Schindler,[63] A. Snyder,[63] D. Su,[63] M. K. Sullivan,[63] J. Va'vra,[63] A. P. Wagner,[63] M. Weaver,[63] W. J. Wisniewski,[63] M. Wittgen,[63] D. H. Wright,[63] H. W. Wulsin,[63] A. K. Yarritu,[63] C. C. Young,[63] V. Ziegler,[63] W. Park,[64] M. V. Purohit,[64] R. M. White,[64] J. R. Wilson,[64] A. Randle-Conde,[65] S. J. Sekula,[65] M. Bellis,[66] J. F. Benitez,[66] P. R. Burchat,[66] T. S. Miyashita,[66] M. S. Alam,[67] J. A. Ernst,[67] R. Gorodeisky,[68] N. Guttman,[68] D. R. Peimer,[68] A. Soffer,[68] P. Lund,[69] S. M. Spanier,[69] R. Eckmann,[70] J. L. Ritchie,[70] A. M. Ruland,[70] C. J. Schilling,[70] R. F. Schwitters,[70] B. C. Wray,[70] J. M. Izen,[71] X. C. Lou,[71] F. Bianchi,[72a,72b] D. Gamba,[72a,72b]

 

L. Lanceri,[73a,73b] L. Vitale,[73a,73b] V. Azzolini,[74] F. Martinez-Vidal,[74] A. Oyanguren,[74] H. Ahmed,[75] J. Albert,[75] Sw. Banerjee,[75] H. H. F. Choi,[75] G. J. King,[75] R. Kowalewski,[75] M. J. Lewczuk,[75] C. Lindsay,[75] I. M. Nugent,[75] J. M. Roney,[75] R. J. Sobie,[75] N. Tasneem,[75] T. J. Gershon,[76] P. F. Harrison,[76] T. E. Latham,[76] E. M. T. Puccio,[76] H. R. Band,[77] S. Dasu,[77] Y. Pan,[77] R. Prepost,[77] and S. L. Wu[77]

(*BABAR* Collaboration)

[1]*Laboratoire d'Annecy-le-Vieux de Physique des Particules (LAPP), Université de Savoie, CNRS/IN2P3, F-74941 Annecy-Le-Vieux, France*
[2]*Universitat de Barcelona, Facultat de Fisica, Departament ECM, E-08028 Barcelona, Spain*
[3a]*INFN Sezione di Bari, I-70126 Bari, Italy*
[3b]*Dipartimento di Fisica, Università di Bari, I-70126 Bari, Italy*
[4]*University of Bergen, Institute of Physics, N-5007 Bergen, Norway*
[5]*Lawrence Berkeley National Laboratory and University of California, Berkeley, California 94720, USA*
[6]*Ruhr Universität Bochum, Institut für Experimentalphysik 1, D-44780 Bochum, Germany*
[7]*University of British Columbia, Vancouver, British Columbia, Canada V6T 1Z1*
[8]*Brunel University, Uxbridge, Middlesex UB8 3PH, United Kingdom*
[9]*Budker Institute of Nuclear Physics, Novosibirsk 630090, Russia*
[10]*University of California at Irvine, Irvine, California 92697, USA*
[11]*University of California at Riverside, Riverside, California 92521, USA*
[12]*University of California at Santa Barbara, Santa Barbara, California 93106, USA*
[13]*University of California at Santa Cruz, Institute for Particle Physics, Santa Cruz, California 95064, USA*
[14]*California Institute of Technology, Pasadena, California 91125, USA*
[15]*University of Cincinnati, Cincinnati, Ohio 45221, USA*
[16]*University of Colorado, Boulder, Colorado 80309, USA*
[17]*Colorado State University, Fort Collins, Colorado 80523, USA*
[18]*Technische Universität Dortmund, Fakultät Physik, D-44221 Dortmund, Germany*
[19]*Technische Universität Dresden, Institut für Kern- und Teilchenphysik, D-01062 Dresden, Germany*
[20]*Laboratoire Leprince-Ringuet, Ecole Polytechnique, CNRS/IN2P3, F-91128 Palaiseau, France*
[21]*University of Edinburgh, Edinburgh EH9 3JZ, United Kingdom*
[22a]*INFN Sezione di Ferrara, I-44100 Ferrara, Italy*
[22b]*Dipartimento di Fisica, Università di Ferrara, I-44100 Ferrara, Italy*
[23]*INFN Laboratori Nazionali di Frascati, I-00044 Frascati, Italy*
[24a]*INFN Sezione di Genova, I-16146 Genova, Italy*
[24b]*Dipartimento di Fisica, Università di Genova, I-16146 Genova, Italy*
[25]*Indian Institute of Technology Guwahati, Guwahati, Assam, 781 039, India*
[26]*Harvard University, Cambridge, Massachusetts 02138, USA*
[27]*Harvey Mudd College, Claremont, California 91711*
[28]*Universität Heidelberg, Physikalisches Institut, Philosophenweg 12, D-69120 Heidelberg, Germany*
[29]*Humboldt-Universität zu Berlin, Institut für Physik, Newtonstrasse 15, D-12489 Berlin, Germany*
[30]*Imperial College London, London, SW7 2AZ, United Kingdom*
[31]*University of Iowa, Iowa City, Iowa 52242, USA*
[32]*Iowa State University, Ames, Iowa 50011-3160, USA*
[33]*Johns Hopkins University, Baltimore, Maryland 21218, USA*
[34]*Laboratoire de l'Accélérateur Linéaire, IN2P3/CNRS et Université Paris-Sud 11, Centre Scientifique d'Orsay, B. P. 34, F-91898 Orsay Cedex, France*
[35]*Lawrence Livermore National Laboratory, Livermore, California 94550, USA*
[36]*University of Liverpool, Liverpool L69 7ZE, United Kingdom*
[37]*Queen Mary, University of London, London, E1 4NS, United Kingdom*
[38]*University of London, Royal Holloway and Bedford New College, Egham, Surrey TW20 0EX, United Kingdom*
[39]*University of Louisville, Louisville, Kentucky 40292, USA*
[40]*Johannes Gutenberg-Universität Mainz, Institut für Kernphysik, D-55099 Mainz, Germany*
[41]*University of Manchester, Manchester M13 9PL, United Kingdom*
[42]*University of Maryland, College Park, Maryland 20742, USA*
[43]*University of Massachusetts, Amherst, Massachusetts 01003, USA*
[44]*Massachusetts Institute of Technology, Laboratory for Nuclear Science, Cambridge, Massachusetts 02139, USA*
[45]*McGill University, Montréal, Québec, Canada H3A 2T8*
[46a]*INFN Sezione di Milano, I-20133 Milano, Italy*

[46b]Dipartimento di Fisica, Università di Milano, I-20133 Milano, Italy
[47]University of Mississippi, University, Mississippi 38677, USA
[48]Université de Montréal, Physique des Particules, Montréal, Québec, Canada H3C 3J7
[49a]INFN Sezione di Napoli, I-80126 Napoli, Italy
[49b]Dipartimento di Scienze Fisiche, Università di Napoli Federico II, I-80126 Napoli, Italy
[50]NIKHEF, National Institute for Nuclear Physics and High Energy Physics, NL-1009 DB Amsterdam, The Netherlands
[51]University of Notre Dame, Notre Dame, Indiana 46556, USA
[52]Ohio State University, Columbus, Ohio 43210, USA
[53]University of Oregon, Eugene, Oregon 97403, USA
[54a]INFN Sezione di Padova, I-35131 Padova, Italy
[54b]Dipartimento di Fisica, Università di Padova, I-35131 Padova, Italy
[55]Laboratoire de Physique Nucléaire et de Hautes Energies, IN2P3/CNRS, Université Pierre et Marie Curie-Paris6, Université Denis Diderot-Paris7, F-75252 Paris, France
[56a]INFN Sezione di Perugia, I-06100 Perugia, Italy
[56b]Dipartimento di Fisica, Università di Perugia, I-06100 Perugia, Italy
[57a]INFN Sezione di Pisa, I-56127 Pisa, Italy
[57b]Dipartimento di Fisica, Università di Pisa, I-56127 Pisa, Italy
[57c]Scuola Normale Superiore di Pisa, I-56127 Pisa, Italy
[58]Princeton University, Princeton, New Jersey 08544, USA
[59a]INFN Sezione di Roma, I-00185 Roma, Italy
[59b]Dipartimento di Fisica, Università di Roma La Sapienza, I-00185 Roma, Italy
[60]Universität Rostock, D-18051 Rostock, Germany
[61]Rutherford Appleton Laboratory, Chilton, Didcot, Oxon, OX11 0QX, United Kingdom
[62]CEA, Irfu, SPP, Centre de Saclay, F-91191 Gif-sur-Yvette, France
[63]SLAC National Accelerator Laboratory, Stanford, California 94309 USA
[64]University of South Carolina, Columbia, South Carolina 29208, USA
[65]Southern Methodist University, Dallas, Texas 75275, USA
[66]Stanford University, Stanford, California 94305-4060, USA
[67]State University of New York, Albany, New York 12222, USA
[68]Tel Aviv University, School of Physics and Astronomy, Tel Aviv, 69978, Israel
[69]University of Tennessee, Knoxville, Tennessee 37996, USA
[70]University of Texas at Austin, Austin, Texas 78712, USA
[71]University of Texas at Dallas, Richardson, Texas 75083, USA
[72a]INFN Sezione di Torino, I-10125 Torino, Italy
[72b]Dipartimento di Fisica Sperimentale, Università di Torino, I-10125 Torino, Italy
[73a]INFN Sezione di Trieste, I-34127 Trieste, Italy
[73b]Dipartimento di Fisica, Università di Trieste, I-34127 Trieste, Italy
[74]IFIC, Universitat de Valencia-CSIC, E-46071 Valencia, Spain
[75]University of Victoria, Victoria, British Columbia, Canada V8W 3P6
[76]Department of Physics, University of Warwick, Coventry CV4 7AL, United Kingdom
[77]University of Wisconsin, Madison, Wisconsin 53706, USA

(Received 5 December 2011; published 7 August 2012)

We report measurements of partial branching fractions for inclusive charmless semileptonic $B$ decays $\bar{B} \to X_u \ell \bar{\nu}$ and the determination of the Cabibbo–Kobayashi–Maskawa (CKM) matrix element $|V_{ub}|$. The analysis is based on a sample of $467 \times 10^6$ $\Upsilon(4S) \to B\bar{B}$ decays recorded with the *BABAR* detector at the PEP-II $e^+e^-$ storage rings. We select events in which the decay of one of the $B$ mesons is fully reconstructed and an electron or a muon signals the semileptonic decay of the other $B$ meson. We measure partial branching fractions $\Delta\mathcal{B}$ in several restricted regions of phase space and determine the CKM element $|V_{ub}|$ based on different QCD predictions. For decays with a charged lepton momentum $p_\ell^* > 1.0$ GeV in the $B$ meson rest frame, we obtain $\Delta\mathcal{B} = (1.80 \pm 0.13_{\text{stat}} \pm 0.15_{\text{sys}} \pm 0.02_{\text{theo}}) \times 10^{-3}$ from a fit to the two-dimensional $M_X - q^2$ distribution. Here, $M_X$ refers to the invariant mass of the final state hadron $X$ and $q^2$ is the invariant mass squared of the charged lepton and neutrino. From this measurement

*Now at Temple University, Philadelphia, PA 19122, USA.
†Also with Università di Perugia, Dipartimento di Fisica, Perugia, Italy.
‡Now at the University of Huddersfield, Huddersfield HD1 3DH, United Kingdom.
§Now at University of South Alabama, Mobile, AL 36688, USA.
‖Also with Università di Sassari, Sassari, Italy.

we extract $|V_{ub}| = (4.33 \pm 0.24_{\rm exp} \pm 0.15_{\rm theo}) \times 10^{-3}$ as the arithmetic average of four results obtained from four different QCD predictions of the partial rate. We separately determine partial branching fractions for $\bar{B}^0$ and $B^-$ decays and derive a limit on the isospin breaking in $\bar{B} \to X_u \ell \bar{\nu}$ decays.

DOI: 10.1103/PhysRevD.86.032004 PACS numbers: 13.20.He, 12.15.Hh, 12.38.Qk, 14.40.Nd

## I. INTRODUCTION

A principal physics goal of the *BABAR* experiment is to establish *CP* violation in *B* meson decays and to test whether the observed effects are consistent with the standard model (SM) expectations. In the SM, *CP*-violating effects result from an irreducible phase in the Cabibbo–Kobayashi–Maskawa (CKM) quark-mixing matrix [1,2]. Precise determinations of the magnitude of the matrix element $|V_{ub}|$ will permit more stringent tests of the SM mechanism for *CP* violation. This is best illustrated in terms of the unitarity triangle [3], the graphical representation of one of the unitarity conditions of the CKM matrix, for which the side opposite to the angle $\beta$ is proportional to the ratio $|V_{ub}|/|V_{cb}|$. The best way to determine $|V_{ub}|$ is to measure the decay rate for $\bar{B} \to X_u \ell \bar{\nu}$ (here $X$ refers to a hadronic final state and the index $c$ or $u$ indicates whether this state carries charm or not), which is proportional to $|V_{ub}|^2$.

There are two approaches to these measurements, based on either inclusive or exclusive measurements of semileptonic decays. The experimental uncertainties on the methods are largely independent, and the extraction of $|V_{ub}|$ from the measured branching fractions relies on different sets of calculations of the hadronic contributions to the matrix element. For quite some time, the results of measurements of $|V_{ub}|$ from inclusive and exclusive decays have been only marginally consistent [4,5]. Global fits [6,7] testing the compatibility of the measured angles and sides with the unitarity triangle of the CKM matrix reveal small differences that might indicate potential deviations from SM expectations. Therefore, it is important to perform redundant and improved measurements, employing different experimental techniques and a variety of theoretical calculations, to better assess the accuracy of the theoretical and experimental uncertainties.

Although inclusive branching fractions exceed those of individual exclusive decays by an order of magnitude, the most challenging task for inclusive measurements is the discrimination between the rare charmless signal and the much more abundant decays involving charmed mesons. To improve the signal-to-background ratio, the events are restricted to selected regions of phase space. Unfortunately these restrictions lead to difficulties in calculating partial branching fractions. They impact the convergence of heavy quark expansions (HQE) [8,9], enhance perturbative and nonperturbative QCD corrections, and thus lead to significantly larger theoretical uncertainties in the determination of $|V_{ub}|$.

We report herein measurements of partial branching fractions ($\Delta\mathcal{B}$) for inclusive charmless semileptonic *B* meson decays, $\bar{B} \to X_u \ell \bar{\nu}$ [10]. This analysis extends the event selection and methods employed previously by *BABAR* to a larger data set [11]. We tag $\Upsilon(4S) \to B\bar{B}$ events with a fully reconstructed hadronic decay of one of the *B* mesons ($B_{\rm reco}$). This technique results in a low event selection efficiency, but it uniquely determines the momentum and charge of both *B* mesons in the event, reducing backgrounds significantly. For charged *B* mesons it also determines their flavor. The semileptonic decay of the second *B* meson ($B_{\rm recoil}$) is identified by the presence of an electron or a muon and its kinematics are constrained such that the undetectable neutrino can be identified from the missing momentum and energy of the rest of the event. However, undetected and poorly reconstructed charged particles or photons lead to large backgrounds from the dominant $\bar{B} \to X_c \ell \bar{\nu}$ decays, and they distort the kinematics, e.g., the hadronic mass $M_X$ and the leptonic mass squared $q^2$.

For the $B_{\rm reco}$ sample, the two dominant background sources are non-$B\bar{B}$ events from continuum processes, $e^+e^- \to q\bar{q}(\gamma)$ with $q = u$, $d$, $s$, or $c$, and combinatorial $B\bar{B}$ background. The sum of these two backgrounds is estimated from the distribution of the beam energy-substituted mass $m_{\rm ES}$, which takes the following form in the laboratory frame: $m_{\rm ES} = \sqrt{(s/2 + \vec{p}_B \cdot \vec{p}_{\rm beams})^2/E^2_{\rm beams} - \vec{p}^{\,2}_B}$. Here $\vec{p}_B$ refers to the momentum of the $B_{\rm reco}$ candidate derived from the measured momenta of its decay products, $P_{\rm beams} = (E_{\rm beams}, \vec{p}_{\rm beams})$ to the four-momentum of the colliding beam particles, and $\sqrt{s}$ to the total energy in the $\Upsilon(4S)$ frame. For correctly reconstructed $B_{\rm reco}$ decays, the distribution peaks at the *B* meson mass, and the width of the peak is determined by the energy spread of the colliding beams. The size of the underlying background is determined from a fit to the $m_{\rm ES}$ distribution.

We minimize experimental systematic uncertainties, by measuring the yield for selected charmless semileptonic decays relative to the total yield of semileptonic decays $\bar{B} \to X \ell \bar{\nu}$, after subtracting combinatorial backgrounds of the $B_{\rm reco}$ selection from both samples.

In order to reduce the overall uncertainties, measurement of the signal $\bar{B} \to X_u \ell \bar{\nu}$ decays is restricted to regions of phase space where the background from the dominant $\bar{B} \to X_c \ell \bar{\nu}$ decays is suppressed and theoretical uncertainties can be reliably assessed. Specifically, signal events tend to have higher charged lepton momenta in the *B*-meson rest frame ($p^*_\ell$), lower $M_X$, higher $q^2$, and smaller values of the light-cone momentum $P_+ = E_X - |\vec{p}_X|$,

where $E_X$ and $\vec{p}_X$ are energy and momentum of the hadronic system $X$ in the $B$ meson rest frame.

The observation of charged leptons with momenta exceeding the kinematic limit for $\bar{B} \to X_c \ell \bar{\nu}$ presented first evidence for charmless semileptonic decays. This was followed by a series of measurements close to this kinematic limit [12–16]. Although the signal-to-background ratio for this small region of phase space is favorable, the theoretical uncertainties are large and difficult to quantify. Since then, efforts have been made to select larger phase space regions, thereby reducing the theoretical uncertainties. The Belle Collaboration has recently published an analysis that covers about 88% of the signal phase space [17], similar to one of the studies detailed in this article.

We extract $|V_{ub}|$ from the partial branching fractions relying on four different QCD calculations of the partial decay rate in several phase space regions: BLNP by Bosch, Lange, Neubert, and Paz [18–20]; DGE, the dressed gluon exponentiation by Andersen and Gardi [21,22]; ADFR by Aglietti, Di Lodovico, Ferrera, and Ricciardi [23,24]; and GGOU by Gambino, Giordano, Ossola, and Uraltsev [25]. These calculations differ significantly in their treatment of perturbative corrections and the parametrization of nonperturbative effects that become important for the different restrictions in phase space.

This measurement of $|V_{ub}|$ is based on combined samples of charged and neutral $B$ mesons. In addition, we present measurements of the partial decay rates for $\bar{B}^0$ and $B^-$ decays separately. The observed rates are found to be equal within uncertainties. We use this observation to set a limit on weak annihilation (WA), the process $b\bar{u} \to \ell^- \bar{\nu}_\ell$, which is not included in the QCD calculation of the $\bar{B} \to X \ell \bar{\nu}$ decay rates. Since final state hadrons originate from soft gluon emission, WA is expected to contribute to the decay rate at large values of $q^2$ [26–29].

The outline of this paper is as follows: a brief overview of the *BABAR* detector, particle reconstruction, and the data and Monte Carlo (MC) samples is given in Sec. II, followed in Sec. III by a description of the event reconstruction and selection of the two event samples, the charmless semileptonic signal sample, and the inclusive semileptonic sample that serves as normalization. The measurement of the partial branching fractions and their systematic uncertainties are presented in Secs. IV and V. The extraction of $|V_{ub}|$ based on four sets of QCD calculations for seven selected regions of phase space is presented in Sec. VI, followed by the conclusions in Sec. VII.

## II. DATA SAMPLE, DETECTOR, AND SIMULATION

### A. Data sample

The data used in this analysis were recorded with the *BABAR* detector at the PEP-II asymmetric energy $e^+e^-$ collider operating at the $\Upsilon(4S)$ resonance. The total data sample, corresponding to an integrated luminosity of 426 fb$^{-1}$ and containing $467 \times 10^6$ $\Upsilon(4S) \to B\bar{B}$ events, was analyzed.

### B. The *BABAR* detector

The *BABAR* detector and the general event reconstruction are described in detail elsewhere [30,31]. For this analysis, the most important detector features are the charged-particle tracking, photon reconstruction, and particle identification. The momenta and angles of charged particles are measured in a tracking system consisting of a five-layer silicon vertex tracker (SVT) and a 40-layer, small-cell drift chamber (DCH). Charged particles of different masses are distinguished by their ionization energy loss in the tracking devices and by the DIRC, a ring-imaging detector of internally reflected Cherenkov radiation. A finely segmented electromagnetic calorimeter (EMC) consisting of 6580 CsI(Tl) crystals measures the energy and position of showers generated by electrons and photons. The EMC is surrounded by a thin superconducting solenoid providing a 1.5 T magnetic field and by a steel flux return with a hexagonal barrel section and two end caps. The segmented flux return (IFR) is instrumented with multiple layers of resistive plate chambers and limited streamer tubes to identify muons and to a lesser degree $K_L$.

### C. Single particle reconstruction

In order to reject misidentified and background tracks that do not originate from the interaction point, we require the radial and longitudinal impact parameters to be $r_0 < 1.5$ cm and $|z_0| < 10$ cm. For secondary tracks from $K_S \to \pi^+\pi^-$ decays, no restrictions on the impact parameter are imposed. The efficiency for the reconstruction of charged particles inside the fiducial volume for SVT, DCH, and EMC, defined by the polar angle in the laboratory frame, $0.410 < \theta_{\rm lab} < 2.54$ rad, exceeds 96% and is well reproduced by MC simulation.

Electromagnetic showers are detected in the EMC as clusters of energy depositions. Photons are required not to be matched to a charged track extrapolated to the position of the shower maximum in the EMC. To suppress photons from beam-related background, we only retain photons with energies larger than 50 MeV. Clusters created by neutral hadrons ($K_L$ or neutrons) interacting in the EMC are distinguished from photons by their shower shape.

Electrons are primarily separated from charged hadrons on the basis of the ratio of the energy deposited in the EMC to the track momentum. This quantity should be close to 1 for electrons since they deposit all their energy in the calorimeter. Most other charged tracks are minimum ionizing, unless they shower in the EMC crystals.

Muons are identified by a neural network that combines information from the IFR with the measured track momentum and the energy deposition in the EMC.

The average electron efficiency for laboratory momenta above 0.5 GeV is 93%, largely independent of momentum.

The average hadron misidentification rate is less than 0.2%. Within the polar-angle acceptance, the average muon efficiency rises with laboratory momentum and reaches a plateau of about 70% above 1.4 GeV. The muon efficiency varies between 50% and 80% as a function of the polar angle. The average hadron misidentification rate is about 1.5%, varying by about 0.5% as a function of momentum and polar angle.

Charged kaons are selected on the basis of information from the DIRC, DCH, and SVT. The efficiency is higher than 80% over most of the momentum range and varies with the polar angle. The probability of a pion to be misidentified as a kaon is close to 2%, varying by about 1% as a function of momentum and polar angle.

Neutral pions are reconstructed from pairs of photon candidates that are detected in the EMC and are assumed to originate from the primary vertex. Photon pairs having an invariant mass within 17.5 MeV (corresponding to $2.5\sigma$) of the nominal $\pi^0$ mass are considered $\pi^0$ candidates. The overall detection efficiency, including solid angle restrictions, varies between 55% and 65% for $\pi^0$ energies in the range of 0.2 to 2.5 GeV.

$K^0_S \to \pi^+\pi^-$ decays are reconstructed as pairs of tracks of opposite charge with a common vertex displaced from the interaction point. The invariant mass of the pair is required to be in the range $490 < m_{\pi^+\pi^-} < 505$ MeV.

### D. Monte Carlo simulation

We use MC techniques to simulate the response of the *BABAR* detector [32] and the particle production and decays [33], to optimize selection criteria, and to determine signal efficiencies and background distributions. The agreement of the simulated distributions with those in data has been verified with control samples, as shown in Sec. IV D; the impact of the inaccuracies of the simulation is estimated in Sec. V.

The size of the simulated sample of generic $B\bar{B}$ events exceeds the $B\bar{B}$ data sample by about a factor of 3. This sample includes the common $\bar{B} \to X_c \ell \bar{\nu}$ decays. MC samples for inclusive and exclusive $\bar{B} \to X_u \ell \bar{\nu}$ decays exceed the size of the data samples by factors of 15 or more.

Charmless semileptonic $\bar{B} \to X_u \ell \bar{\nu}$ decays are simulated as a combination of resonant three-body decays with $X_u = \pi$, $\eta$, $\eta'$, $\rho$, $\omega$, and decays to nonresonant hadronic final states $X_u$. The branching ratios assumed for the various resonant decays are detailed in Table I. Exclusive charmless semileptonic decays are simulated using a number of different parametrizations: for $\bar{B} \to \pi \ell \bar{\nu}$ decays we use a single-pole ansatz [35] for the $q^2$ dependence of the form factor with a single parameter measured by *BABAR* [36]; for decays to pseudoscalar mesons $\eta$ and $\eta'$ and vector mesons $\rho$ and $\omega$ we use form factor parametrizations based on light-cone sum calculations [37,38].

TABLE I. Branching fractions and their uncertainties [34] for exclusive $\bar{B} \to X_u \ell \bar{\nu}$ decays.

| Mode | $\mathcal{B}(\bar{B}^0 \to X_u \ell \bar{\nu})$ | $\mathcal{B}(B^- \to X_u \ell \bar{\nu})$ |
|---|---|---|
| $\bar{B} \to \pi \ell \bar{\nu}$ | $(136 \pm 7) \times 10^{-6}$ | $(77 \pm 12) \times 10^{-6}$ |
| $\bar{B} \to \eta \ell \bar{\nu}$ | | $(64 \pm 20) \times 10^{-6}$ |
| $\bar{B} \to \rho \ell \bar{\nu}$ | $(247 \pm 33) \times 10^{-6}$ | $(128 \pm 18) \times 10^{-6}$ |
| $\bar{B} \to \omega \ell \bar{\nu}$ | | $(115 \pm 17) \times 10^{-6}$ |
| $\bar{B} \to \eta' \ell \bar{\nu}$ | | $(17 \pm 22) \times 10^{-6}$ |

The simulation of the inclusive charmless semileptonic $B$ decays to hadronic states with masses larger than $2m_\pi$ is based on a prescription by De Fazio and Neubert (DFN) [39] for the triple-differential decay rate, $d^3\Gamma/dq^2 dE_\ell ds_H$ ($E_\ell$ refers to the energy of the charged lepton and $s_H = M_X^2$) with QCD corrections up to $\mathcal{O}(\alpha_s)$. The motion of the $b$ quark inside the $B$ meson is incorporated in the DFN formalism by convolving the parton-level triple-differential decay rate with a nonperturbative shape function (SF). This SF describes the distribution of the momentum $k_+$ of the $b$ quark inside the $B$ meson. The two free parameters of the SF are $\bar{\Lambda}^{\rm SF}$ and $\lambda_1{}^{\rm SF}$. The first relates the $B$ meson mass $m_B$ to the $b$ quark mass, $m_b^{\rm SF} = m_B - \bar{\Lambda}^{\rm SF}$, and $\lambda_1{}^{\rm SF}$ is the average momentum squared of the $b$ quark. The SF parametrization is of the form $F(k_+) = N(1-x)^a e^{(1+a)x}$, where $x = k_+/\bar{\Lambda}^{\rm SF} \le 1$ and $a = -3(\bar{\Lambda}^{\rm SF})^2/\lambda_1{}^{\rm SF} - 1$. The first three moments $A_i$ of the SF must satisfy the following relations: $A_0 = 1, A_1 = 0$, and $A_2 = -\lambda_1{}^{\rm SF}/3$.

The nonresonant hadronic state $X_u$ is simulated with a continuous invariant mass spectrum according to the DFN prescription. The fragmentation of the $X_u$ system into final state hadrons is performed by JETSET [40]. The resonant and nonresonant components are combined such that the sum of their branching fractions is equal to the measured branching fraction for inclusive $\bar{B} \to X_u \ell \bar{\nu}$ decays [34], and the spectra agree with the DFN prediction. In order to obtain predictions for different values of $\bar{\Lambda}^{\rm SF}$ and $\lambda_1{}^{\rm SF}$, the generated events are reweighted.

We estimate the shape of background distributions by using simulations of the process $e^+e^- \to \Upsilon(4S) \to B\bar{B}$ with the $B$ mesons decaying according to measured branching fractions [34].

For the simulation of the dominant background from $\bar{B} \to X_c \ell \bar{\nu}$ decays, we have chosen a variety of different form factor parametrizations. For $\bar{B} \to D \ell \bar{\nu}$ and $\bar{B} \to D^* \ell \bar{\nu}$ decays we use parametrizations [41] based on heavy quark effective theory [42–45]. In the limit of negligible charged lepton masses, decays to pseudoscalar mesons are described by a single form factor for which the $q^2$ dependence is expressed in terms of a slope parameter $\rho_D^2$. We use the world average $\rho_D^2 = 1.19 \pm 0.06$ [46], updated with recent precise measurements by the *BABAR* Collaboration [47,48]. Decays to vector mesons are

described by three form factors, of which the axial vector form factor dominates. In the limit of heavy quark symmetry, their $q^2$ dependence can be described by three parameters for which we use the most precise *BABAR* measurements [47,49]: $\rho^2_{D*} = 1.20 \pm 0.04$ [47,49], $R_1 = 1.429 \pm 0.074$, and $R_2 = 0.827 \pm 0.044$ [49]. For the simulation of semileptonic decays to the four $L = 1$ charm states, commonly referred to as $D^{**}$ resonances, we use calculations of form factors by Leibovich, Ligeti, Stewart, and Wise [50]. We have adopted the prescription by Goity and Roberts [51] for nonresonant $\bar{B} \to D^{(*)} X \ell \bar{\nu}$ decays.

## III. EVENT RECONSTRUCTION AND SIGNAL EXTRACTION

### A. Reconstruction of hadronic $B$ decays tagging $B\bar{B}$ events

$\Upsilon(4S) \to B\bar{B}$ events are tagged by the hadronic decays of one of the $B$ mesons based on a semiexclusive algorithm that was employed in an earlier analysis [11]. We look for decays of the type $B_{\rm reco} \to D^{(*)} Y^{\pm}$, where $D^{(*)}$ is a charmed meson ($D^0$, $D^+$, $D^{*0}$, or $D^{*\pm}$) and $Y$ is a charged state decaying into at most five charged hadrons (pions or kaons), plus at most two neutral mesons ($K^0_S$ or $\pi^0$). The following decay modes of $D$ mesons are reconstructed: $D^0 \to K^-\pi^+$, $K^-\pi^+\pi^0$, $K^-\pi^+\pi^-\pi^+$, $K^0_S\pi^+\pi^-$ and $D^+ \to K^-\pi^+\pi^+$, $K^-\pi^+\pi^+\pi^0$, $K^0_S\pi^+$, $K^0_S\pi^+\pi^+\pi^-$, $K^0_S\pi^+\pi^0$ with $K^0_S \to \pi^+\pi^-$. $D^*$ mesons are identified by their decays, $D^{*+} \to D^0\pi^+$, $D^+\pi^0$ and $D^{*0} \to D^0\pi^0$, $D^0\gamma$. Pions and photons from $D^*$ decays are of low energy, and therefore the mass difference $\Delta M = m(D\pi) - m(D)$ serves as an excellent discriminator for these decays.

Of the 1113 $B_{\rm reco}$ decay chains that we consider, we retain only the 342 ones with a signal purity $\mathcal{P} = S/(S+B) > 20\%$, where $S$ and $B$, derived from MC samples, denote the signal and background yields. The kinematic consistency of the $B_{\rm reco}$ candidates with $B$ meson decays is checked using $m_{\rm ES}$ and the energy difference, $\Delta E = (P_B \cdot P_{\rm beams} - s/2)/\sqrt{s}$. We restrict the $B_{\rm reco}$ mass to $m_{\rm ES} > 5.22$ GeV and require $\Delta E = 0$ GeV within approximately 3 standard deviations, where the $\Delta E$ resolution depends on the decay chain. If an event contains more than one $B_{\rm reco}$ candidate, the decay chain with the highest $\chi^2$ probability is chosen. For this purpose we define

$$\chi^2_{\rm total} = \chi^2_{\rm vertex} + \left(\frac{M_{D^{(*)}_{\rm reco}} - M_{D^{(*)}}}{\sigma_{D^{(*)}_{\rm reco}}}\right)^2 + \left(\frac{\Delta E}{\sigma_{\Delta E}}\right)^2. \quad (1)$$

Here the first term is taken from a vertex fit for tracks from $B_{\rm reco}$ decays, the second relates reconstructed and nominal masses [34], $M_{D^{(*)}_{\rm reco}}$ and $M_{D^{(*)}}$, of the charm mesons ($D^0$, $D^+$, $D^{*0}$, or $D^{*\pm}$), with the resolution $\sigma_{D^{(*)}_{\rm reco}}$, and the third term checks the energy balance $\Delta E$ compared to its resolution $\sigma_{\Delta E}$. The number of degrees of freedom is therefore defined as $N^{\rm dof} = N^{\rm dof}_{\rm vertex} + 2$. The resulting overall tagging efficiency is 0.3% for $B^0\bar{B}^0$ and 0.5% for $B^+B^-$ events.

### B. Selection of inclusive $\bar{B} \to X\ell\bar{\nu}$ decays

In order to minimize systematic uncertainties, we measure the yield of selected charmless semileptonic decays in a specific kinematic region normalized to the total yield of semileptonic $\bar{B} \to X\ell\bar{\nu}$ decays. Both semileptonic decays, the charmless and the normalization modes, are identified by at least one charged lepton in events that are tagged by a $B_{\rm reco}$ decay. Both samples are background-subtracted and corrected for efficiency. Using this normalization, the systematic uncertainties on the $B_{\rm reco}$ reconstruction and the charged lepton detection cancel in the ratio or are eliminated to a large degree.

The selection criteria for the charmless and the total semileptonic samples are chosen to minimize the statistical uncertainty of the measurement as estimated from a sample of fully simulated MC events that includes both signal and background processes.

A restriction on the momentum of the electron or muon is applied to suppress backgrounds from secondary charm or $\tau^{\pm}$ decays, photon conversions, and misidentified hadrons. This is applied to $p^*_\ell$, the lepton momentum in the rest frame of the recoiling $B$ meson, which is accessible since the momenta of the $\Upsilon(4S)$ and the reconstructed $B$ are known. This transformation is important because theoretical calculations refer to variables that are Lorentz invariant or measured in the rest frame of the decaying $B$ meson. We require $p^*_\ell$ to be greater than 1 GeV, for which about 90% of the signal is retained.

For electrons and muons the angular acceptance is defined as $0.450 < \theta < 2.473$ rad, where $\theta$ refers to the polar angle relative to the electron beam in the laboratory frame. This requirement excludes regions where charged-particle tracking and identification are not efficient. We suppress muons from $J/\psi$ decays by rejecting the event if a muon candidate paired with any other charged track of opposite charge (and not part of $B_{\rm reco}$) results in an invariant mass of the pair that is consistent with the $J/\psi$ mass. A similar requirement is not imposed on electron candidates, because of the poor resolution of the corresponding $J/\psi$ peak.

We also reject events if the electron candidate paired with any other charged track of opposite charge is consistent with a $\gamma \to e^+e^-$ conversion.

A variety of processes contributes to the inclusive semileptonic event samples, i.e. candidates selected by a $B_{\rm reco}$ decay and the presence of a high momentum lepton. In addition to true semileptonic decays tagged by a correctly reconstructed $B_{\rm reco}$, we consider the following classes of backgrounds:

(i) *Combinatorial background:* the $B_{\rm reco}$ is not correctly reconstructed. This background originates from $B\bar{B}$ or continuum $e^+e^- \to q\bar{q}(\gamma)$ events. In order to

subtract this background, the yield of true $B_{\rm reco}$ decays is determined from an unbinned maximum-likelihood fit to the $m_{\rm ES}$ distribution (Sec. III D).

(ii) *Cascade background:* the lepton does not originate from a semileptonic $B$ decay, but from secondary decays, for instance, from $D$ mesons, including $D_s \to \tau\nu$, or residual $J/\psi$ background.

(iii) $\tau$ *background:* electrons or muons originate from prompt $\tau$ leptons, primarily from $\bar{B} \to X\tau\bar{\nu}$ decays.

(iv) *Fake leptons:* hadrons are misidentified as leptons, primarily muons.

The last three sources of background are combined and in the following are referred to as "other" background.

### C. Selection of inclusive $\bar{B} \to X_u \ell \bar{\nu}$ decays

A large fraction of $\bar{B} \to X_c \ell \bar{\nu}$ decays is expected to have a second lepton from cascade decays of the charm particles. In contrast, in $\bar{B} \to X_u \ell \bar{\nu}$ decays secondary leptons are very rare. Therefore, we enhance signal events by selecting events with only one charged lepton having $p^*_\ell > 1$ GeV.

In semileptonic $B$ meson decays, the charge of the primary lepton is equal to the sign of the charge of the $b$ quark. Thus for $B^+B^-$ events in which the $B_{\rm reco}$ and the lepton originate from different $B$ decays in the event, we impose the requirement $Q_b Q_\ell < 0$, where $Q_b$ is the charge of the $b$ quark of the $B_{\rm reco}$ and $Q_\ell$ is the charge of the lepton. For $B^0\bar{B}^0$ events this condition does not strictly hold because of flavor mixing. Thus, to avoid a loss in efficiency, this requirement is not imposed. The hadronic state $X_u$ in charmless semileptonic decays is reconstructed from all particles that are not associated with the $B_{\rm reco}$ candidate or the charged lepton. The measured four-momentum $P_X$ is defined as

$$P_X = \sum_{i=1}^{N_{\rm trk}} P_i^{\rm trk} + \sum_{i=1}^{N_\gamma} P_i^\gamma, \qquad (2)$$

where the summation extends over the four-vectors of the charged particles and photon candidates. From this four-vector, other kinematic variables, $M_X^2 = P_X^2 = E_X^2 - p_X^2$, $q^2 = P_{B_{\rm reco}} - P_X$ ($P_{B_{\rm reco}}$ being the $B_{\rm reco}$ four-momentum), and $P_+$, can be calculated. The loss of one or more charged or neutral particles or the addition of tracks or single electrons from photon conversions degrade the reconstruction of $X_u$ and the resolution of the measurement of any related kinematic variables. In order to reduce the impact of missing charged particles and the effect of single electrons from $\gamma \to e^+e^-$ conversions, we impose charge conservation on the whole event, $Q_{\rm tot} = Q_{B_{\rm reco}} + Q_X + Q_\ell = 0$. This requirement rejects a larger fraction of $\bar{B} \to X_c \ell \bar{\nu}$ events because of their higher charged multiplicity and the presence of very low momentum charged pions from $D^{*\pm} \to D^0 \pi^\pm_{\rm soft}$ decays that have low detection efficiency.

In $\bar{B} \to X\ell\bar{\nu}$ decays, where the state $X$ decays hadronically, the only undetected particle is a neutrino. The neutrino four-momentum $P_\nu$ can be estimated from the missing momentum four-vector $P_{\rm miss} = P_{\Upsilon(4S)} - P_{B_{\rm reco}} - P_X - P_\ell$. For correctly reconstructed events with a single semileptonic decay, the missing mass squared, $MM^2 = P^2_{\rm miss}$, is consistent with zero. Failure to detect one or more particles in the event creates a tail at large positive values; thus $MM^2$ is used as a measure of the quality of the event reconstruction. Though $MM^2$ is Lorentz invariant, the missing momentum is usually measured in the laboratory frame, because this avoids the additional uncertainty related to the transformation into the c.m. frame. We require $MM^2$ to be less than 0.5 GeV$^2$. Because of the higher probability for additional unreconstructed neutral particles, a neutrino, or $K_L$, the $MM^2$ distribution is broader for $\bar{B} \to X_c \ell \bar{\nu}$ decays, and this restriction suppresses this background more than signal events.

In addition, we suppress the $\bar{B} \to D^* \ell \bar{\nu}$ background by exploiting the small $Q$ value of the $D^* \to D\pi_{\rm soft}$ decays, which result in a very low momentum pion. For energetic $D^*$ mesons, the momenta $p_{\pi_{\rm soft}}$ and $p_D$ are almost collinear, and we can approximate the $D^*$ direction by the $\pi_{\rm soft}$ direction and estimate the $D^*$ energy by a simple approximation based on the $E_{\pi_{\rm soft}}$, $E_{D^*} \approx m_{D^*} \times E_{\pi_{\rm soft}}/145$ MeV. Using the measured $B_{\rm reco}$ and charged lepton momenta, and the four-momentum of the $D^*$ derived from any pion with c.m. momentum below 200 MeV, we estimate the neutrino mass for a potential $\bar{B} \to D^* \ell \bar{\nu}$ decay as $MM^2_{\rm veto} = (P_B - P_{D^*} - P_\ell)^2$. For true $\bar{B} \to D^* \ell \bar{\nu}$ decays, this distribution peaks at zero. Thus, we veto $D^*$ decays to low momentum charged or neutral pions by requiring, respectively, $MM^2_{\rm veto}(\pi^+_{\rm soft}) < -3$ GeV$^2$ or $MM^2_{\rm veto}(\pi^0_{\rm soft}) < -2$ GeV$^2$. This is achieved without explicit reconstruction of the $D$ meson decays, and thus avoids large losses in rejection power for this veto.

We reduce $\bar{B} \to D^* \ell \bar{\nu}$ background by vetoing events with a charged or neutral kaon ($K^0_S \to \pi^+\pi^-$) that originate primarily from the decays of charm particles.

A summary of the impact of the signal selection criteria on the high-energy lepton sample, for the signal, semileptonic, and nonsemileptonic background samples is presented in Table II, in terms of cumulative selection efficiencies. Figure 1 shows the kinematic variables that appear in Table II for different event categories. Combinatorial background is not included; it is subtracted based on fits to the $m_{\rm ES}$ distributions, as described in Sec. III D. The overall efficiency for selecting charmless semileptonic decays in the sample of tagged events with a charged lepton is 33.8%; the background reduction is 97.8% for $\bar{B} \to X_c \ell \bar{\nu}$ and 95.3% for "other."

The resolution functions determined from MC simulation of signal events passing the selection requirements are

TABLE II. Comparison of the cumulative selection efficiencies for samples of signal $\bar{B} \to X_u \ell \bar{\nu}$ decays and $\bar{B} \to X_c \ell \bar{\nu}$ and "other" backgrounds. The efficiencies are relative to the sample of $B_{\rm reco}$-tagged events with a charged lepton.

| Selection | $\bar{B} \to X_u \ell \bar{\nu}$ | $\bar{B} \to X_c \ell \bar{\nu}$ | Other |
|---|---|---|---|
| Only one lepton | 99.3% | 98.1% | 95.8% |
| Total charge $Q = 0$ | 65.5% | 52.9% | 49.1% |
| $MM^2$ | 44.2% | 17.8% | 17.8% |
| $D^* \ell \bar{\nu}(\pi_s^+)$ veto | 40.6% | 9.9% | 14.4% |
| $D^* \ell \bar{\nu}(\pi_s^0)$ veto | 34.8% | 6.3% | 9.1% |
| Kaon veto | 33.8% | 2.2% | 4.7% |

shown in Fig. 2 for the variables $M_X$, $q^2$, and $P_+$. Each of these distributions has a narrow core containing 30%, 50%, and 30% of the $\bar{B} \to X_u \ell \bar{\nu}$ events, with widths of 25 MeV, 250 MeV$^2$, and 10 MeV, respectively. The remaining events have a considerably poorer resolution, primarily because of lost secondary particles from the decay of the hadronic $X_u$.

On the basis of the kaon and the $D^*$ veto, two data samples are defined:

(i) *signal-enriched:* events that pass the vetoes; this sample is used to extract the signal;

(ii) *signal-depleted:* events rejected by at least one veto; they are used as the control sample to check the agreement between data and simulated backgrounds, including the poorly understood $\bar{B} \to D^{**} \ell \bar{\nu}$ decays.

### D. Subtraction of combinatorial background

The subtraction of the combinatorial background of the $B_{\rm reco}$ tag for the signal and normalization samples relies on unbinned maximum-likelihood fits to the $m_{\rm ES}$ distributions. For signal decays the goal is to extract the distributions in the kinematic variables $p_\ell^*$, $M_X$, $q^2$, and $P_+$. Because the shapes and relative yields of the signal and background contributions depend on the values of these kinematic variables, the continuum and combinatorial background subtraction is performed separately for subsamples corresponding to events in bins of these variables. This results in more accurate spectra than a single fit to the full sample of events in each selected region of phase space.

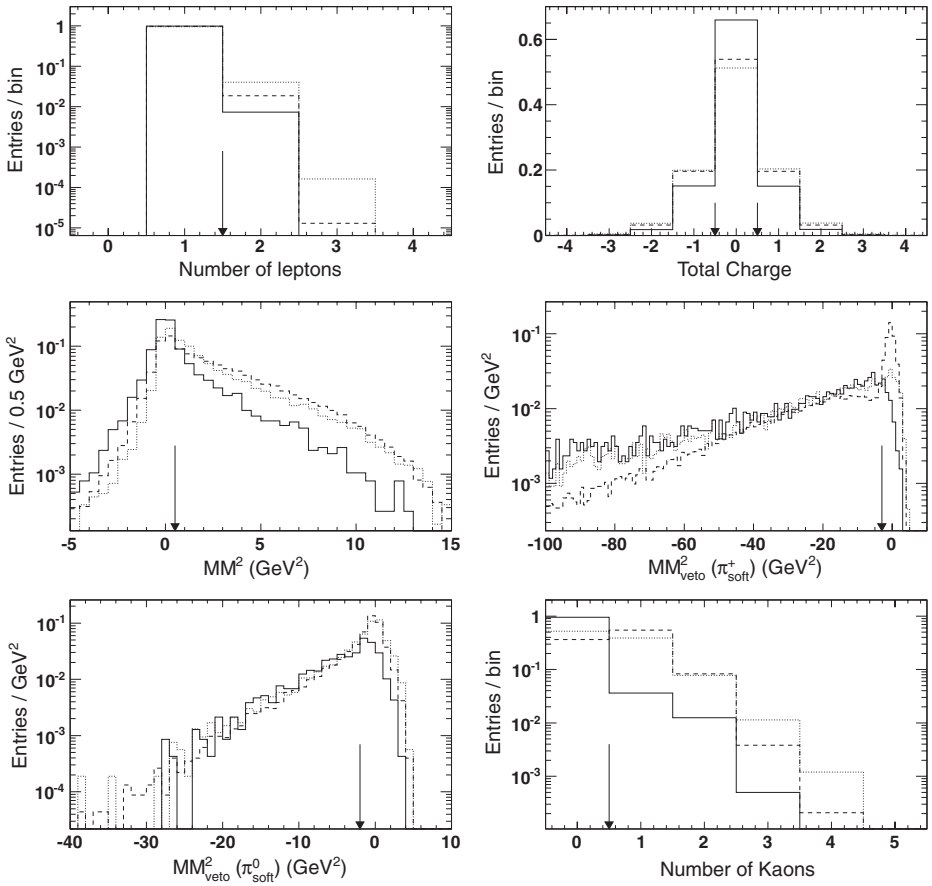


FIG. 1. MC distribution of the kinematic variables for which we apply restrictions sequentially as listed in Table II, for $\bar{B} \to X_u \ell \bar{\nu}$ (solid line), $\bar{B} \to X_c \ell \bar{\nu}$ (dashed line), and "other" component (dotted line). All distributions are normalized to unity, and selection criteria have been applied cumulatively, except those affecting directly the variable shown. The arrows indicate the selection requirement for a specific variable, as described in Sec. III C.

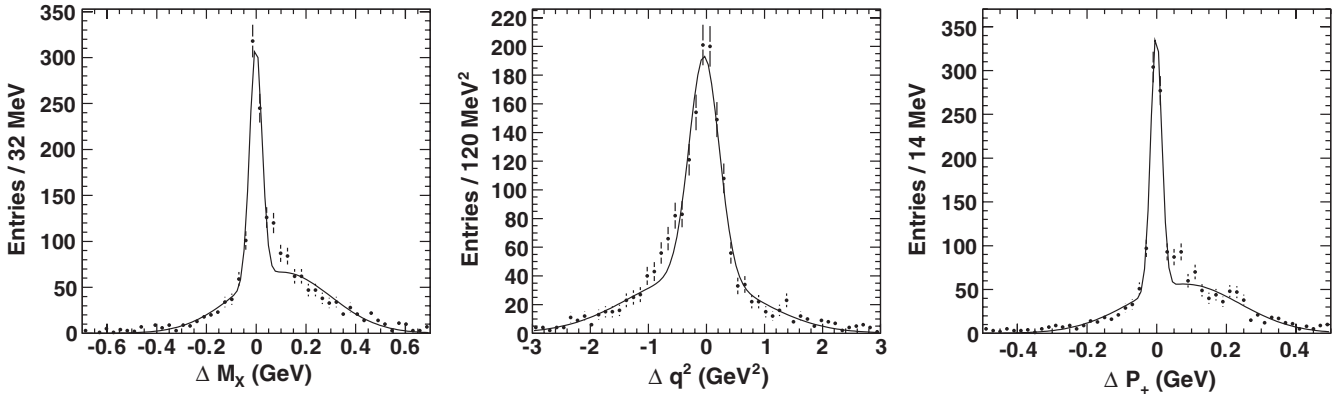


FIG. 2. Resolution for MC simulated for signal $\bar{B} \to X_u \ell \bar{\nu}$ events passing all event selection criteria, (left) $M_{X\mathrm{reco}} - M_{X\mathrm{true}}$, (center) ${q^2}_{\mathrm{reco}} - {q^2}_{\mathrm{true}}$, and (right) $P_{+,\mathrm{reco}} - P_{+,\mathrm{true}}$. The curve shows a fit result for the sum of two Gaussian functions.

For the normalization sample, the fit is performed for the full event sample, separately for $\bar{B}^0$ and $B^-$ tags.

The $m_{\mathrm{ES}}$ distribution for the combinatorial $B_{\mathrm{reco}}$ background can be described by an ARGUS function [52],

$$f_{\mathrm{bkg}}(m) = N_{\mathrm{bkg}} m \sqrt{1-m^2}\, e^{-\xi(1-m^2)}, \tag{3}$$

where $m = m_{\mathrm{ES}}/m_{\mathrm{ES}}^{\mathrm{max}}$ and $m_{\mathrm{ES}}^{\mathrm{max}}$ is the end point of the $m_{\mathrm{ES}}$ distribution that depends on the beam energy, and $\xi$ determines the shape of the function. $N_{\mathrm{bkg}}$ refers to the total number of background events in the distribution.

For signal events, the $m_{\mathrm{ES}}$ distribution resembles a resolution function peaking at the $B$ meson mass with a slight tail to lower masses. Usually the peak of the $m_{\mathrm{ES}}$ distribution is empirically described by a crystal ball function [53], but this ansatz turned out to be inadequate for this data set because the $B_{\mathrm{reco}}$ sample is composed of many individual decay modes with different resolutions. We therefore follow an approach previously used in *BABAR* data [54] and build a more general function, using a Gaussian function, $f_g(x) = e^{-x^2/2}$, and the derivative of $\tanh x$, $f_t(x) = e^{-x}/(1+e^{-x})$, to arrive at

$$f_{\mathrm{sig}}(\Delta) = \begin{cases} \frac{C_2}{(C_3-\Delta)^n} & \text{if } \Delta < \alpha \\ \frac{C_1}{\sigma_L} f_t\left(\frac{\Delta}{\sigma_L}\right) & \text{if } \alpha \le \Delta < 0 \\ \frac{r}{\sigma_1} f_t\left(\frac{\Delta}{\sigma_1}\right) + \frac{1-r}{\sigma_2} f_g\left(\frac{\Delta}{\sigma_2}\right) & \text{if } \Delta \ge 0 \end{cases}. \tag{4}$$

Here $\Delta = m_{\mathrm{ES}} - \bar{m}_{\mathrm{ES}}$, where $\bar{m}_{\mathrm{ES}}$ is the maximum of the $m_{\mathrm{ES}}$ distribution. $C_1$, $C_2$, and $C_3$ are functions of the parameters $\bar{m}_{\mathrm{ES}}$, $r$, $\sigma_1$, $\sigma_2$, $\sigma_L$, $\alpha$, and $n$, which ensure the continuity of $f_{\mathrm{sig}}$.

Given the very large number of parameters, we first perform a fit to samples covering the full kinematic range and determine all parameters describing $f_{\mathrm{sig}}$ and the ARGUS function. We then repeat the fit for events in each bin of the kinematic variables, with only the relative normalization of the signal and background, and the shape parameter $\xi$ of the ARGUS function as free parameters. Figure 3 shows the $m_{\mathrm{ES}}$ distribution for the inclusive semileptonic sample, separately for charged and neutral $B$ mesons.

Finally, we correct for the contamination from cascade background in the number of neutral $B$ mesons, due to the effect of $B^0 - \bar{B}^0$ mixing, in each bin of the kinematic variables. We distinguish neutral $B$ decays with right- and wrong-sign leptons, based on the flavor of the $B_{\mathrm{reco}}$ decay. The contribution from cascade decays is subtracted by computing the number of neutral $B$ mesons $N_{B^0}$ as

$$N_{B^0} = \frac{1-\chi_d}{1-2\chi_d} N_{B^0_{\mathrm{rs}}} - \frac{\chi_d}{1-2\chi_d} N_{B^0_{\mathrm{ws}}}, \tag{5}$$

where $N_{B^0_{\mathrm{rs}}}$ and $N_{B^0_{\mathrm{ws}}}$ are the number of neutral $B$ mesons with right and wrong sign of the charge of the accompanying lepton, and $\chi_d = 0.188 \pm 0.002$ [34] is the $B^0 - \bar{B}^0$ mixing parameter.

The performance of the $m_{\mathrm{ES}}$ fit has been verified using MC simulated distributions. We split the full sample in two parts. One part, containing one-third of the events, is treated as data and is similar in size to the total data sample.

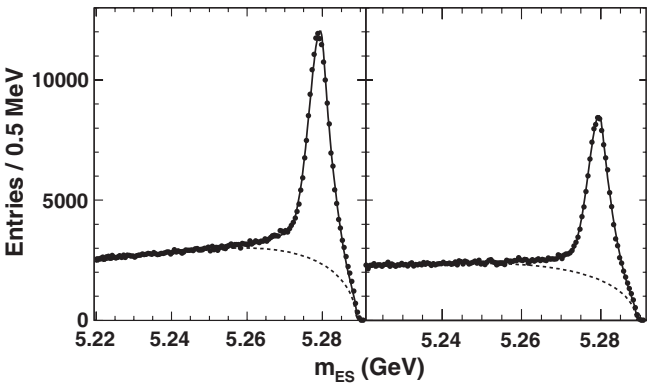


FIG. 3. The $m_{\mathrm{ES}}$ distribution for the inclusive semileptonic sample, for fully reconstructed hadronic decays of $B^-$ (left) and $\bar{B}^0$ mesons (right). The solid line shows the result of the maximum-likelihood fit to signal and combinatorial backgrounds; the dashed line indicates the shape of the background described by an ARGUS function.

The remaining two-thirds represent the simulation. The fit procedure, described in Sec. IV, is applied to these samples and yields, within uncertainties, the charmless semileptonic branching fraction that is input to the MC generation.

## IV. SIGNAL EXTRACTION AND PARTIAL BRANCHING FRACTION MEASUREMENT

### A. Signal yield

Once continuum and combinatorial $B\bar{B}$ backgrounds have been subtracted and the mixing correction has been applied, the resulting differential distributions of the kinematic variables are fitted using a $\chi^2$ minimization to extract $N_u$, the number of selected signal events. The $\chi^2$ for these fits is defined as

$$\chi^2 = \sum_i \frac{[N^i - (C_{\rm sig} N_u^{i,\rm MC} + C_{\rm bkg} N_{\rm bkg}^{i,\rm MC})]^2}{\sigma(N^i)^2 + \sigma(N^{i,\rm MC})^2}, \qquad (6)$$

where, for each bin $i$ of variable width, $N^i$ is the number of observed events, and $N_u^{i,\rm MC}$ and $N_{\rm bkg}^{i,\rm MC}$ are the number of MC predicted events for signal and background, respectively. The statistical uncertainties $\sigma(N^i)$ and $\sigma(N^{i,\rm MC})$ are taken from fits to the $m_{\rm ES}$ distributions in data and MC simulations. The scale factors $C_{\rm sig}$ and $C_{\rm bkg}$ are free parameters of the fit. The differential distributions are compared with the sum of the signal and background distributions resulting from the fit in Figs. 4 and 5. For the $\bar{B} \to X_u \ell \bar{\nu}$ signal contributions we distinguish between decays that were generated with values of the kinematic variable inside the restricted phase space regions and a small number of events, $N_u^{\rm out}$, with values outside these regions. This distinction allows us to relate the fitted signal yields to the theoretical calculations applied to extract $|V_{ub}|$.

### B. Partial branching fractions

We obtain partial branching fractions for charmless semileptonic decays from the observed number of signal events in the kinematic regions considered, after correction for background and efficiency, and normalization to the total number of semileptonic decays $\bar{B} \to X \ell \bar{\nu}$ observed in the $B_{\rm reco}$ event sample. For each of the restricted regions of phase space under study, we calculate the ratio

$$\Delta R_{\rm u/sl} = \frac{\Delta \mathcal{B}(\bar{B} \to X_u \ell \bar{\nu})}{\mathcal{B}(\bar{B} \to X \ell \bar{\nu})} = \frac{N_u^{\rm true}}{N_{\rm sl}^{\rm true}} = \frac{(N_u)/(\epsilon_{\rm sel}^u \epsilon_{\rm kin}^u)}{(N_{\rm sl} - BG_{\rm sl})} \frac{\epsilon_\ell^{\rm sl} \epsilon_{\rm tag}^{\rm sl}}{\epsilon_\ell^u \epsilon_{\rm tag}^u}. \qquad (7)$$

Here, $N_u^{\rm true}$ and $N_{\rm sl}^{\rm true}$ refer to the true number of signal and normalization events. The observed signal yield $N_u$ is related to $N_u^{\rm true}$ by $N_u = \epsilon_{\rm sel}^u \epsilon_{\rm kin}^u \epsilon_l^u \epsilon_{\rm tag}^u N_u^{\rm true}$, where $\epsilon_{\rm sel}^u$ is the efficiency for detecting $\bar{B} \to X_u \ell \bar{\nu}$ decays in the tagged sample after applying all selection criteria, $\epsilon_{\rm kin}$ is the fraction of signal events with both true and reconstructed $M_X$, $P_+$, $q^2$, or $p_\ell^*$ within the restricted region of phase space, and $\epsilon_l^u$ refers to the efficiency for selecting a lepton from a $\bar{B} \to X_u \ell \bar{\nu}$ decay with a momentum $p_\ell^* > 1$ GeV in a signal event tagged with efficiency $\epsilon_{\rm tag}^u$. Similarly, $N_{\rm sl}^{\rm true}$ is related to $N_{\rm sl}$, the fitted number of observed $B_{\rm reco}$ accompanied by a charged lepton with $p_\ell^* > 1$ GeV, through $N_{\rm sl}^{\rm true} = (N_{\rm sl} - BG_{\rm sl})/\epsilon_\ell^{\rm sl} \epsilon_{\rm tag}^{\rm sl}$. Here, $BG_{\rm sl}$ is the remaining peaking background estimated from MC simulation, $N_{\rm sl}$ is obtained from the $m_{\rm ES}$ fit to the selected semileptonic sample, and $\epsilon_\ell^{\rm sl}$ refers to the efficiency for selecting a lepton from a semileptonic $B$ decay with a momentum $p_\ell^* > 1$ GeV in an event

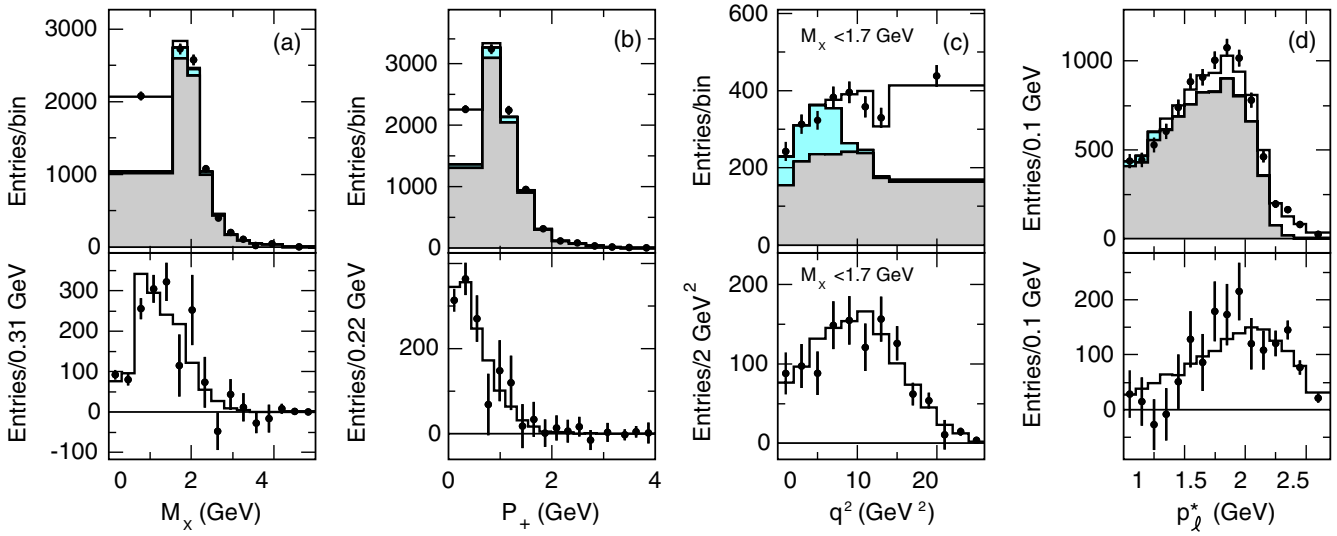


FIG. 4 (color online). Measured distributions (data points) of (a) $M_X$, (b) $P_+$, (c) $q^2$ with $M_X < 1.7$ GeV, and (d) $p_\ell^*$. Upper row: comparison with the result of the $\chi^2$ fit with varying bin size for the sum of two scaled MC contributions (histograms), $\bar{B} \to X_u \ell \bar{\nu}$ decays generated inside (white) or outside (light shading) the selected kinematic region, and the background (dark shading). Lower row: corresponding spectra with equal bin size after background subtraction based on the fit. The data are not corrected for efficiency.

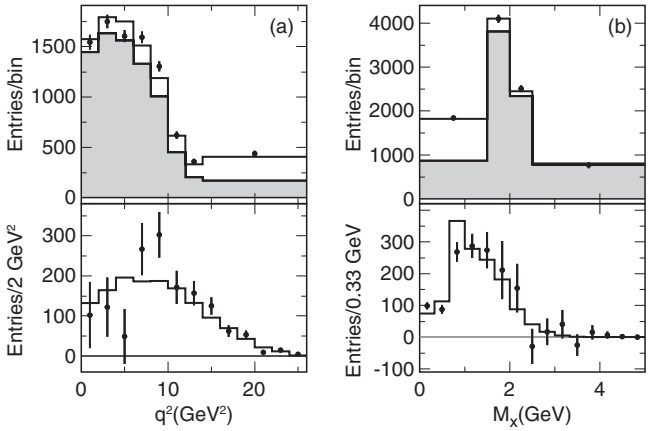


FIG. 5. Projections of measured distributions (data points) of (a) $q^2$ and (b) $M_X$ with varying bin size, for the fit to the $M_X - q^2$ distribution without constraints other than $p^*_\ell > 1$ GeV. Upper row: comparison with the result of the $\chi^2$ fit to the two-dimensional $M_X - q^2$ distribution for the sum of two scaled MC contributions (histograms), $\bar{B} \to X_u \ell \bar{\nu}$ decays (white), and the background (dark shading). Lower row: corresponding spectra with equal bin size after background subtraction based on the fit. The data are not corrected for efficiency.

tagged with efficiency $\epsilon^{\rm sl}_{\rm tag}$. We obtain $N_{\rm sl} = 237,433 \pm 838$ and $BG_{\rm sl} = 20,705 \pm 132$.

The ratio of efficiencies in Eq. (7) accounts for differences in the final states and the different lepton momentum spectra for the two classes of events, and their impact on the tagging. The efficiencies for $B_{\rm reco}$ tagging and lepton detection are not very different, and thus the efficiency ratio is close to 1.

We convert Eq. (7) to partial branching fractions by using the total semileptonic branching fraction, $\mathcal{B}(\bar{B} \to X \ell \bar{\nu}) = (10.75 \pm 0.15)\%$ [34].

The regions of phase space, fitted event yields, efficiencies introduced in Eq. (7), and partial branching fractions are listed in Table III; the regions are one-dimensional in $M_X$, $P_+$, or $p^*_\ell$, or two-dimensional in the plane $M_X$ versus $q^2$. In the following, we will refer to the latter as $M_X - q^2$. Two fits have been performed with no additional kinematic restrictions, apart from the requirement $p^*_\ell > 1$ GeV: a fit to the lepton momentum spectrum and a fit to the two-dimensional histogram $M_X - q^2$. Since the same events enter both fits, the correlation is very high. The fact that the results are in excellent agreement indicates that the distribution of the simulated signal and background distributions agree well with the data.

Correlations between the different analyses are reported in the entries above the main diagonal of Table IV.

In addition, a series of fits to the lepton momentum spectrum has been performed with the lower limit on $p^*_\ell$ increasing from 1.0 GeV to 2.4 GeV. The results are presented in Sec. VI; the measurement at $p^*_\ell > 1.3$ GeV gives the smallest total uncertainty and is also quoted in Table III.

TABLE III. List of the fitted numbers of signal events $N_u$, the number of events generated outside the kinematic selection $N^{\rm out}_u$, the efficiencies, the partial branching fractions $\Delta\mathcal{B}(\bar{B} \to X_u \ell \bar{\nu})$, and the $\chi^2$ per degree of freedom for the different selected regions of phase space. The first uncertainty is statistical, the second systematic. The $p^*_\ell > 1$ GeV requirement is implicitly assumed.

| Region of phase space | $N_u$ | $N^{\rm out}_u$ | $\epsilon^u_{\rm sel}\epsilon^u_{\rm kin}$ | $(\epsilon^{\rm sl}_\ell \epsilon^{\rm sl}_t)/(\epsilon^u_\ell \epsilon^u_t)$ | $\Delta\mathcal{B}(\bar{B} \to X_u \ell \bar{\nu})(10^{-3})$ | $\chi^2$/ndof |
|---|---|---|---|---|---|---|
| $M_X < 1.55$ GeV | $1033 \pm 73$ | $29 \pm 2$ | $0.365 \pm 0.002$ | $1.29 \pm 0.03$ | $1.08 \pm 0.08 \pm 0.06$ | 7.9/8 |
| $M_X < 1.70$ GeV | $1089 \pm 82$ | $25 \pm 2$ | $0.370 \pm 0.002$ | $1.27 \pm 0.04$ | $1.15 \pm 0.10 \pm 0.08$ | 6.6/8 |
| $P_+ < 0.66$ GeV | $902 \pm 80$ | $54 \pm 5$ | $0.375 \pm 0.003$ | $1.22 \pm 0.03$ | $0.98 \pm 0.09 \pm 0.08$ | 3.4/9 |
| $M_X < 1.70$ GeV, $q^2 > 8$ GeV$^2$ | $665 \pm 53$ | $39 \pm 3$ | $0.386 \pm 0.003$ | $1.25 \pm 0.03$ | $0.68 \pm 0.06 \pm 0.04$ | 23.7/26 |
| $M_X - q^2$ | $1441 \pm 102$ | 0 | $0.338 \pm 0.002$ | $1.18 \pm 0.03$ | $1.80 \pm 0.13 \pm 0.15$ | 31.0/29 |
| $p^*_\ell > 1.0$ GeV | $1470 \pm 130$ | $8 \pm 2$ | $0.342 \pm 0.002$ | $1.18 \pm 0.03$ | $1.81 \pm 0.16 \pm 0.19$ | 21.6/14 |
| $p^*_\ell > 1.3$ GeV | $1329 \pm 121$ | $61 \pm 5$ | $0.363 \pm 0.002$ | $1.18 \pm 0.09$ | $1.53 \pm 0.13 \pm 0.14$ | 20.4/14 |

TABLE IV. Correlation coefficients for measurements in different kinematic regions. The entries above the main diagonal refer to correlations (statistical and systematic) for pairs of measurements of the partial branching fractions; the entries below the diagonal refer to the correlations (experimental and theoretical) for pairs of $|V_{ub}|$ measurements.

| Phase space restriction | $M_X < 1.55$ GeV | $M_X < 1.70$ GeV | $P_+ < 0.66$ GeV | $M_X < 1.70$ GeV, $q^2 > 8$ GeV$^2$ | $M_X - q^2$ $p^*_\ell > 1.0$ GeV | $p^*_\ell > 1.3$ GeV |
|---|---|---|---|---|---|---|
| $M_X < 1.55$ GeV | 1 | 0.77 | 0.74 | 0.50 | 0.72 | 0.57 |
| $M_X < 1.70$ GeV | 0.81 | 1 | 0.86 | 0.55 | 0.94 | 0.73 |
| $P_+ < 0.66$ GeV | 0.69 | 0.81 | 1 | 0.46 | 0.78 | 0.61 |
| $M_X < 1.70$ GeV, $q^2 > 8$ GeV$^2$ | 0.40 | 0.46 | 0.38 | 1 | 0.52 | 0.46 |
| $M_X - q^2$ | 0.58 | 0.88 | 0.67 | 0.34 | 1 | 0.74 |
| $p^*_\ell > 1.3$ GeV | 0.53 | 0.72 | 0.58 | 0.40 | 0.72 | 1 |

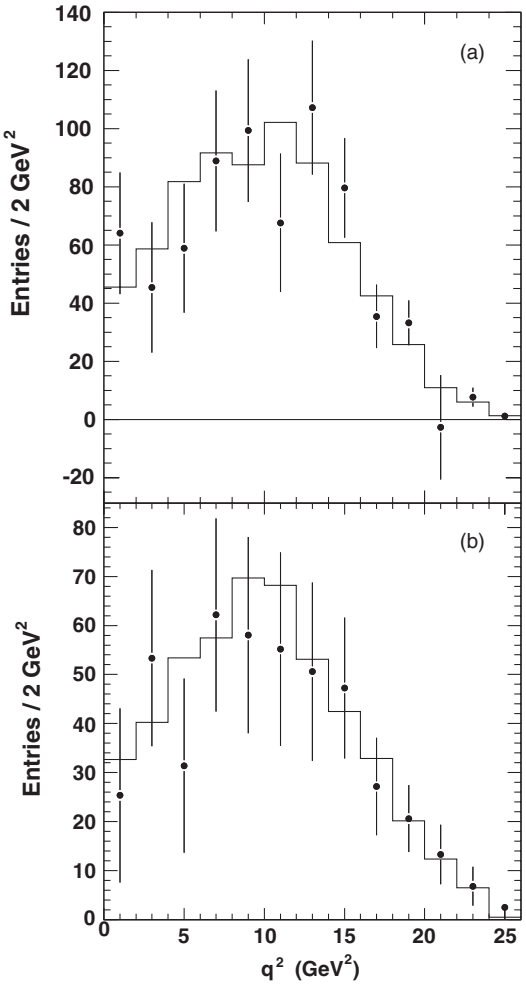


FIG. 6. Comparison of the measured $q^2$ distributions (data points) for $M_X < 1.7$ GeV for charmless semileptonic decays of (a) charged and (b) neutral $B$ mesons to the results of the fit (histogram), after $\bar{B} \to X_c \ell \bar{\nu}$ and "other" background subtraction.

Consistency checks have been performed. The analyses done on data samples collected in different data-taking periods, or separating the lepton flavor or charge, have all yielded the same results, within experimental uncertainties.

### C. Partial branching fractions for $\bar{B}^0$ and $B^-$

All the fits, except those to the $p_\ell^*$ distribution, have been repeated separately for charged and neutral $B_{\rm reco}$ tags. In this case, we extract the true signal yields from the measurements by the following relations to determine the partial branching fractions:

$$N^0_{\rm meas} = \mathcal{P}_{\bar{B}^0_{\rm true} \to \bar{B}^0_{\rm reco}} N^0_{\rm true} + \mathcal{P}_{B^-_{\rm true} \to \bar{B}^0_{\rm reco}} N^-_{\rm true},$$
$$N^-_{\rm meas} = \mathcal{P}_{\bar{B}^0_{\rm true} \to B^-_{\rm reco}} N^0_{\rm true} + \mathcal{P}_{B^-_{\rm true} \to B^-_{\rm reco}} N^-_{\rm true},$$

where the cross-feed probabilities, $\mathcal{P}_{B^-_{\rm true} \to \bar{B}^0_{\rm reco}}$ and $\mathcal{P}_{\bar{B}^0_{\rm true} \to B^-_{\rm reco}}$, are computed using MC simulated events and are typically of the order of (2–3)%.

Figure 6 shows the $q^2$ distributions of $\bar{B} \to X_u \ell \bar{\nu}$ events after background subtraction, for charged and neutral $B$ decays, with $M_X < 1.7$ GeV. Fitted yields, efficiencies, and partial branching fractions are given in Table V.

### D. Data–Monte Carlo comparisons

The separation of the signal events from the non-combinatorial backgrounds relies heavily on the MC simulation to correctly describe the distribution for signal and background sources. Therefore, an extensive study has been devoted to detailed comparisons of data and MC distributions.

A correction applied to the simulation improves the quality of the fits to the kinematic distributions in regions that are dominated by the $\bar{B} \to X_c \ell \bar{\nu}$ background, especially in the high $M_X$ region. In the simulation, we adjust $\lambda_{D^{**}}$, the ratio of branching fractions of semileptonic decays to $P$-wave $D$ mesons and nonresonant charm states decaying to $D^{(*)}X$, over the sum of all $D^{(*)}\ell\bar{\nu}$ and "other" background components,

$$\lambda_{D^{**}} = \frac{\mathcal{B}(\bar{B} \to D^{**}\ell\bar{\nu}) + \mathcal{B}(\bar{B} \to D^{(*)}X\ell\bar{\nu})}{\mathcal{B}(\bar{B} \to D^{(*)}\ell\bar{\nu}) + \mathcal{B}(\bar{B} \to X_{\rm other})}. \quad (8)$$

TABLE V. Summary of the fits to separate samples of neutral and charged $B$ decays. For details see Table III.

| $\bar{B}^0$ decays | $N_u$ | $N_u^{\rm out}$ | $\epsilon^u_{\rm sel}\epsilon^u_{\rm kin}$ | $(\epsilon^{\rm sl}_\ell \epsilon^{\rm sl}_t)/(\epsilon^u_\ell \epsilon^u_t)$ | $\Delta\mathcal{B}(\bar{B} \to X_u \ell \bar{\nu})(10^{-3})$ | $\chi^2$/ndof |
|---|---|---|---|---|---|---|
| $M_X < 1.55$ GeV | $458 \pm 48$ | $12 \pm 1$ | $0.360 \pm 0.004$ | $1.49 \pm 0.07$ | $1.09 \pm 0.12 \pm 0.11$ | 19.0/9 |
| $M_X < 1.70$ GeV | $444 \pm 53$ | $12 \pm 1$ | $0.370 \pm 0.004$ | $1.45 \pm 0.07$ | $1.12 \pm 0.11 \pm 0.11$ | 16.6/9 |
| $P_+ < 0.66$ GeV | $434 \pm 52$ | $27 \pm 3$ | $0.367 \pm 0.004$ | $1.38 \pm 0.06$ | $1.09 \pm 0.13 \pm 0.11$ | 9.1/9 |
| $M_X < 1.70$ GeV, $q^2 > 8$ GeV$^2$ | $262 \pm 38$ | $16 \pm 2$ | $0.380 \pm 0.005$ | $1.43 \pm 0.06$ | $0.61 \pm 0.09 \pm 0.06$ | 15.8/26 |
| $M_X - q^2$ | $553 \pm 72$ | 0 | $0.328 \pm 0.003$ | $1.36 \pm 0.08$ | $1.58 \pm 0.21 \pm 0.20$ | 14.8/29 |
| $B^-$ decays | $N_u$ | $N_u^{\rm out}$ | $\epsilon^u_{\rm sel}\epsilon^u_{\rm kin}$ | $(\epsilon^{\rm sl}_\ell \epsilon^{\rm sl}_t)/(\epsilon^u_\ell \epsilon^u_t)$ | $\Delta\mathcal{B}(\bar{B} \to X_u \ell \bar{\nu})(10^{-3})$ | $\chi^2$/ndof |
| $M_X < 1.55$ GeV | $591 \pm 56$ | $17 \pm 2$ | $0.370 \pm 0.003$ | $1.18 \pm 0.04$ | $1.12 \pm 0.11 \pm 0.11$ | 3.1/9 |
| $M_X < 1.70$ GeV | $669 \pm 63$ | $14 \pm 1$ | $0.370 \pm 0.003$ | $1.17 \pm 0.07$ | $1.27 \pm 0.14 \pm 0.13$ | 3.3/9 |
| $P_+ < 0.66$ GeV | $491 \pm 61$ | $28 \pm 4$ | $0.379 \pm 0.004$ | $1.11 \pm 0.03$ | $0.96 \pm 0.12 \pm 0.12$ | 2.0/9 |
| $M_X < 1.70$ GeV, $q^2 > 8$ GeV$^2$ | $406 \pm 41$ | $24 \pm 2$ | $0.392 \pm 0.004$ | $1.43 \pm 0.03$ | $0.74 \pm 0.08 \pm 0.08$ | 26.9/26 |
| $M_X - q^2$ | $859 \pm 79$ | 0 | $0.345 \pm 0.003$ | $1.07 \pm 0.03$ | $1.91 \pm 0.18 \pm 0.22$ | 36.7/29 |

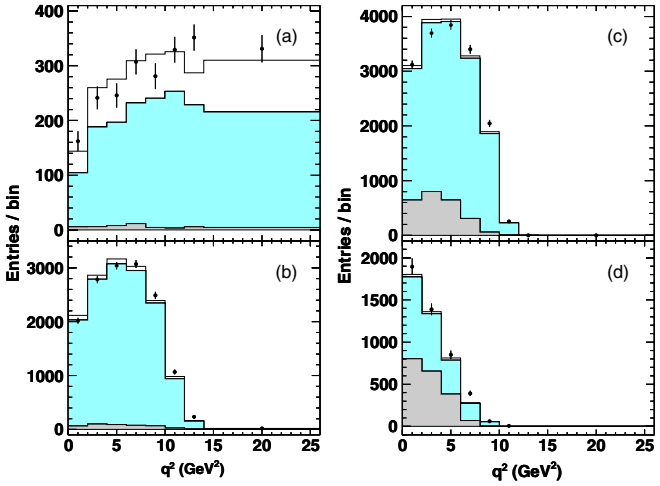


FIG. 7 (color online). Fit results to the $M_X - q^2$ distribution for the signal-depleted sample. The $q^2$ distribution is reported separately for the four $M_X$ bins: (a) $M_X \leq 1.5$ GeV, (b) $1.5 < M_X \leq 2.0$ GeV, (c) $2.0 < M_X \leq 2.5$ GeV, and (d) $2.5 < M_X \leq 3.0$ GeV. The three MC contributions shown here are $\bar{B} \to X_u \ell \bar{\nu}$ decays vetoed by the selection (no shading), $\bar{B} \to D \ell \bar{\nu}$, $\bar{B} \to D^* \ell \bar{\nu}$, and "other" background (light shading), and the $\bar{B} \to D^{**} \ell \bar{\nu}$ component as defined in the text (dark shading).

This ratio has been determined from data by performing a fit on the $M_X - q^2$ distribution of the signal-depleted sample without kinematic selection. The resulting distribution of this fit is shown in Fig. 7. We measure $\lambda_{D^{**}} = 0.73 \pm 0.08$, where the error takes into account the fact that $\chi^2/\text{ndof} = 2$. Other determinations, using signal-enriched samples, give statistically consistent results. This adjustment improves the quality of the fits in regions where backgrounds dominate, but it has a small impact on the fitted signal yield. We have verified that using $D^{**}$ MC correction factors determined separately on each analysis do not change significantly the results with respect to our default strategy, where $\lambda_{D^{**}}$ is determined for the most inclusive sample available, namely, the signal-depleted sample of the analysis without kinematic requirements.

Figures 8 and 9 show comparisons of data and MC distributions, after subtraction of the combinatorial background, for signal-enriched and signal-depleted event samples. All the selection criteria have been applied, except those affecting directly the variable shown. The spectra are background subtracted based on the results of the $m_{\rm ES}$ fit performed for each bin of the variable shown. The uncertainties on data points are on the yields of the bin-by-bin fits. The data and MC distributions are

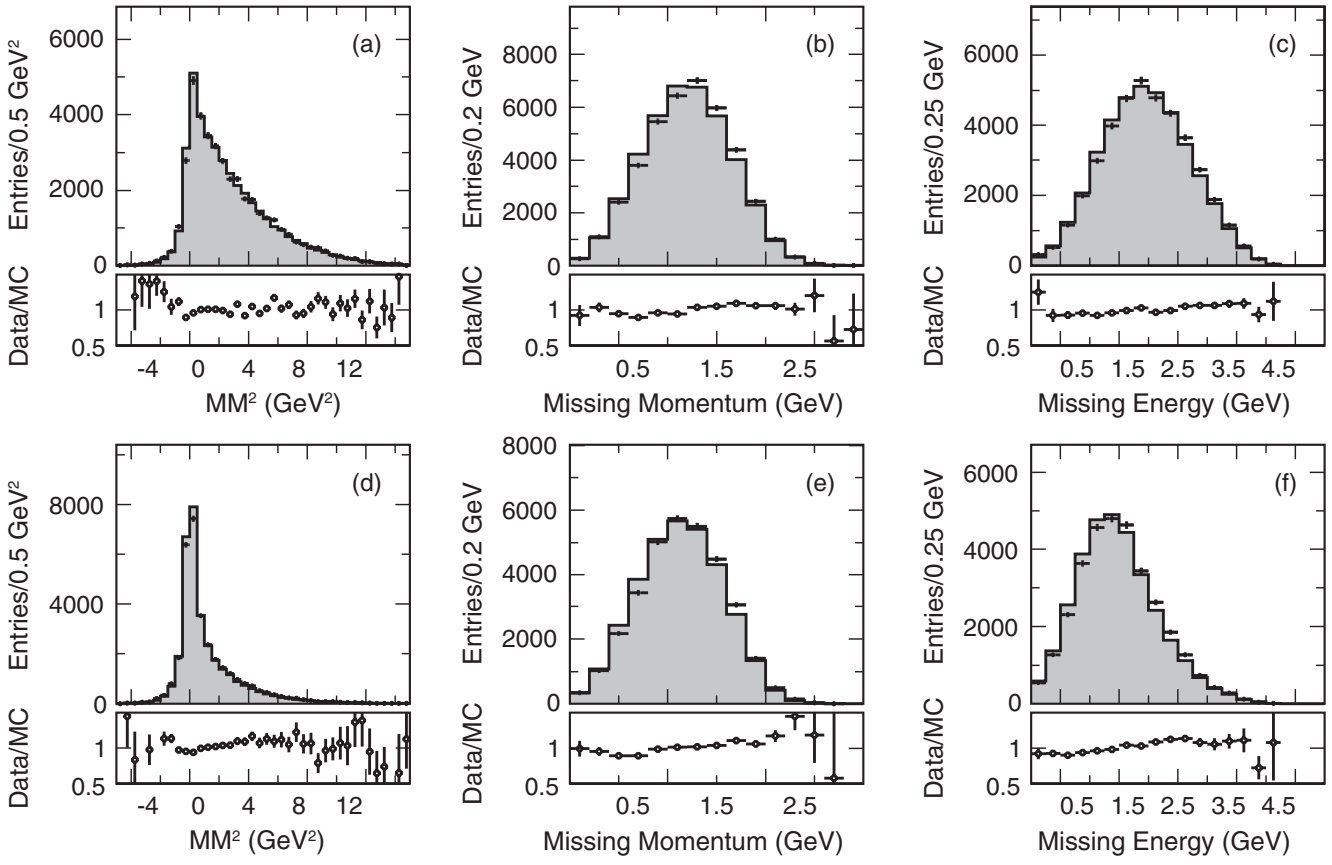


FIG. 8. Comparison of data (points with statistical uncertainties) and MC (histograms) simulated distributions of (a),(d) the missing mass squared, (b),(e) the missing momentum, and (c),(f) the missing energy for $\bar{B} \to X_u \ell \bar{\nu}$ enhanced (top row) and depleted (bottom row) event samples.

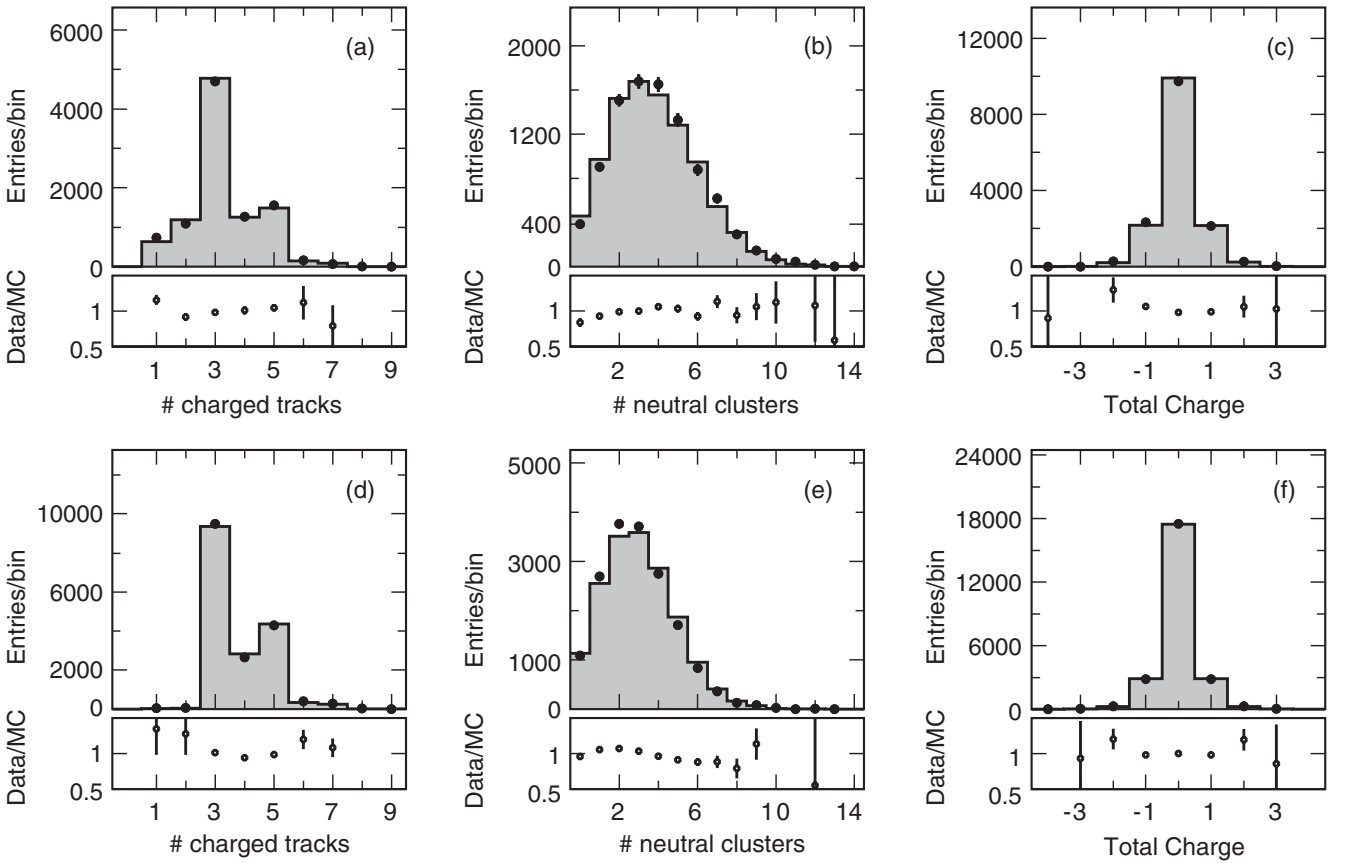


FIG. 9. Comparison of data (points with statistical uncertainties) and MC (histograms) simulated distributions of (a),(d) the charged track multiplicity, (b),(e) the photon multiplicity, and (c),(f) the total charge per event for $\bar{B} \to X_u \ell \bar{\nu}$ enhanced (top row) and depleted (bottom row) event samples.

normalized to the same area. The overall agreement is reasonable, taking into account that the uncertainties are purely statistical. The effects that introduce differences between data and simulation are described in Sec. V; their impact is assessed and accounted for as systematic uncertainty.

## V. SYSTEMATIC UNCERTAINTIES

The experimental technique described in this article, namely, the measurement of a ratio of branching fractions, ensures that systematic uncertainties due, for example, to radiative corrections or differences between $B^{\pm}$ and $B^0$ or $\bar{B}^0$ production rate and lifetime, are negligible. A summary of all other statistical and systematic uncertainties on the partial branching fractions for selected kinematic regions of phase space is shown in Table VI for the complete data sample, and in Table VII for charged and neutral $B$ samples separately.

The individual sources of systematic uncertainties are, to a good approximation, uncorrelated and can therefore be added in quadrature to obtain the total systematic uncertainties for a partial branching fraction. In the following, we discuss the assessment of the systematic uncertainties in detail.

To estimate the systematic uncertainties on the ratio $\Delta R_{u/sl}$, we compare the results obtained from the nominal fits with results obtained after changes to the MC simulation that reflect the uncertainty in the parameters that impact the detector efficiency and resolution or the simulation of signal and background processes. For instance, we lower the tracking efficiency by randomly eliminating a fraction of tracks (corresponding to the estimated uncertainty) in the MC sample, redo the event reconstruction and selection on the recoil side, perform the fit, and take the difference compared to the results obtained with the nominal MC simulation as an estimate of the systematic uncertainty. The sources of systematic uncertainties are largely identical for all selected signal samples, but the size of their impact varies slightly.

### A. Detector effects

Uncertainties in the reconstruction efficiencies for charged and neutral particles, in the rate of tracks and photons from beam background, misreconstructed tracks, failures in the matching of EMC clusters to charged tracks,

TABLE VI. Statistical and systematic uncertainties (in percent) on measurements of the partial branching fraction in seven selected kinematic regions. The total systematic uncertainty is the sum in quadrature of the MC statistical uncertainty and all the other single contributions from detector effects, signal and background simulation, background subtraction, and normalization. The total uncertainty is the sum in quadrature of the data statistical and total systematic uncertainties.

| Phase space restriction | $M_X < 1.55$ GeV | $M_X < 1.70$ GeV | $P_+ < 0.66$ GeV | $M_X < 1.70$ GeV, $q^2 > 8$ GeV$^2$ | $M_X - q^2$ | $p_\ell^* > 1.0$ GeV | $p_\ell^* > 1.3$ GeV |
|---|---|---|---|---|---|---|---|
| Data statistical uncertainty | 7.1 | 8.9 | 8.9 | 8.0 | 7.1 | 9.4 | 8.8 |
| MC statistical uncertainty | 1.3 | 1.3 | 1.3 | 1.6 | 1.1 | 1.1 | 1.2 |
| | | | Detector effects | | | | |
| Track efficiency | 0.4 | 1.0 | 1.1 | 1.7 | 0.7 | 1.2 | 1.0 |
| Photon efficiency | 1.3 | 2.1 | 4.0 | 0.7 | 1.0 | 0.9 | 0.9 |
| $\pi^0$ efficiency | 1.2 | 0.9 | 1.1 | 0.9 | 0.9 | 2.9 | 1.1 |
| Particle identification | 1.9 | 2.4 | 3.3 | 2.9 | 2.3 | 2.9 | 2.2 |
| $K_L$ production/detection | 0.9 | 1.3 | 1.1 | 2.1 | 1.6 | 1.3 | 0.6 |
| $K_S$ production/detection | 0.8 | 1.4 | 1.7 | 2.1 | 1.2 | 1.3 | 0.3 |
| | | | Signal simulation | | | | |
| Shape function parameters | 2.0 | 1.3 | 1.2 | 0.7 | 5.4 | 6.4 | 6.6 |
| Shape function form | 1.2 | 1.6 | 2.6 | 1.2 | 1.5 | 1.1 | 1.1 |
| Exclusive $\bar{B} \to X_u \ell \bar{\nu}$ | 0.6 | 1.3 | 1.6 | 0.7 | 1.9 | 5.3 | 3.4 |
| $s\bar{s}$ production | 1.2 | 1.6 | 1.1 | 1.0 | 2.7 | 3.1 | 2.4 |
| | | | Background simulation | | | | |
| $B$ semileptonic branching ratio | 0.9 | 1.4 | 1.5 | 1.4 | 1.0 | 0.8 | 0.7 |
| $D$ decays | 1.1 | 0.6 | 1.1 | 0.6 | 1.1 | 1.6 | 1.5 |
| $B \to D \ell \nu$ form factor | 0.5 | 0.5 | 1.3 | 0.4 | 0.4 | 0.1 | 0.2 |
| $B \to D^* \ell \nu$ form factor | 0.7 | 0.7 | 0.9 | 0.7 | 0.7 | 0.7 | 0.7 |
| $B \to D^{**} \ell \nu$ form factor | 0.8 | 0.9 | 1.3 | 0.4 | 0.9 | 1.0 | 0.3 |
| $B \to D^{**}$ reweighting | 0.5 | 1.4 | 1.5 | 1.0 | 1.9 | 0.4 | 1.5 |
| | | | $m_{\rm ES}$ background subtraction | | | | |
| $m_{\rm ES}$ background subtraction | 2.0 | 2.7 | 1.9 | 2.6 | 1.9 | 2.0 | 2.5 |
| Combinatorial backg. | 1.8 | 1.8 | 2.6 | 1.8 | 1.0 | 2.1 | 0.5 |
| | | | Normalization | | | | |
| Total semileptonic BF | 1.4 | 1.4 | 1.4 | 1.4 | 1.4 | 1.4 | 1.4 |
| Total systematic uncertainty | 5.5 | 6.7 | 8.3 | 6.6 | 8.4 | 11.0 | 9.3 |
| Total experimental uncertainty | 9.0 | 11.1 | 12.2 | 10.4 | 11.0 | 14.4 | 12.8 |

TABLE VII. Statistical and systematic uncertainties (in percent) on the partial branching fraction for neutral and charged $B$ mesons for the five selected kinematic regions. The total systematic uncertainty is the sum in quadrature of the MC statistical uncertainty and all the other single contributions from detector effects, signal and background simulation, background subtraction, and normalization. The total uncertainty is the sum in quadrature of the data statistical and total systematic uncertainties.

| | $M_X < 1.55$ GeV | | $M_X < 1.70$ GeV | | $P_+ < 0.66$ GeV | | $M_X < 1.70$ GeV, $q^2 > 8$ GeV$^2$ | | $M_X - q^2$ | |
|---|---|---|---|---|---|---|---|---|---|---|
| Phase space restriction | $\bar{B}^0$ | $B^-$ | $\bar{B}^0$ | $B^-$ | $\bar{B}^0$ | $B^-$ | $\bar{B}^0$ | $B^-$ | $\bar{B}^0$ | $B^-$ |
| Data statistical uncertainty | 10.4 | 9.6 | 14.4 | 11.0 | 12.0 | 12.5 | 14.6 | 10.1 | 13.0 | 9.2 |
| MC statistical uncertainty | 2.5 | 1.6 | 2.5 | 1.6 | 2.4 | 1.8 | 2.8 | 2.0 | 1.9 | 1.3 |
| Detector effects | 4.5 | 4.9 | 5.0 | 6.3 | 5.9 | 7.2 | 5.3 | 6.3 | 5.6 | 4.7 |
| Signal simulation | 6.6 | 5.4 | 5.2 | 4.8 | 4.8 | 5.9 | 3.7 | 5.4 | 8.7 | 7.6 |
| Background simulation | 4.4 | 4.2 | 5.6 | 4.5 | 5.9 | 5.4 | 4.9 | 4.4 | 4.4 | 5.0 |
| $m_{\rm ES}$ background subtraction | 4.1 | 5.4 | 5.2 | 5.0 | 2.9 | 5.3 | 5.2 | 5.1 | 3.8 | 4.1 |
| Total semileptonic BF | 1.4 | 1.4 | 1.4 | 1.4 | 1.4 | 1.4 | 1.4 | 1.4 | 1.4 | 1.4 |
| Total systematic uncertainty | 10.4 | 10.2 | 10.9 | 10.6 | 10.5 | 12.2 | 10.1 | 11.0 | 12.1 | 11.2 |
| Total experimental uncertainty | 14.7 | 14.0 | 18.1 | 15.3 | 15.9 | 17.5 | 17.8 | 14.9 | 17.8 | 14.5 |

showers split off from hadronic interactions, undetected $K_L$, and additional neutrinos, all contribute to the event reconstruction and impact the variables that are used in the event selection and the analysis. For all these effects the uncertainties in the efficiencies and resolution have been derived from comparisons of data and MC simulation for selected control samples.

From the study of the angular and momentum distributions of low momentum pions in $D^*$ samples, we estimate the uncertainty on the track finding efficiency at low momenta to be about 1.0%. For all other tracks, the difference between data and MC in tracking efficiency is estimated to be about 0.5% per track. The systematic uncertainty on the ratio $\Delta R_{u/sl}$ is calculated as described above and shown in Tables VI and VII.

Similarly, for single photons, we estimate the systematic uncertainty by randomly eliminating showers that are not matched to the $\pi^0_{\rm soft}$ used to veto $\bar{B} \to D^* \ell \bar{\nu}$ decays, with a probability of 1.8% per shower.

We estimate the systematic uncertainty due to $\pi^0$ detection by randomly eliminating neutral pions that are used in the $\bar{B} \to D^* \ell \bar{\nu}$ veto, with a probability of 3% per $\pi^0$.

Uncertainties on charged-particle identification efficiencies have been assessed to be 2.0% for electrons and 3.0% for muons. The uncertainty on the corresponding misidentification rates are estimated to be 15%. Systematic uncertainties on the kaon identification efficiency and misidentification rate are 2% and 15%, respectively.

In this analysis, no effort was made to identify $K^0_L$. On the other hand, $K^0_L$ mesons interacting in the detector deposit only a fraction of their energy in the EMC, thus they impact $P_{\rm miss}$ and other kinematic variables used in this analysis. Based on detailed studies of data control samples of $D^0 \to K^0 \pi^+ \pi^-$ decays, corrections to the $K^0_L$ efficiency and energy deposition have been derived and applied to the simulation as a function of the $K^0_L$ momentum and angle. We take the difference compared to the results obtained without this correction applied to the simulation as an estimate of the systematic uncertainty.

Differences in both $K^0_L$ and $K^0_S$ production rates of data and MC are taken into account by adjusting the inclusive $D \to K^0 X$ and $D_s \to K^0 X$ branching fractions. The associated systematic uncertainty is assessed by varying these branching fractions within their uncertainties.

## B. Signal and background simulation

### 1. Signal simulation

Knowledge of the details of inclusive $\bar{B} \to X_u \ell \bar{\nu}$ decays is crucial to several aspects of the analysis: the fraction of events within the selected kinematic region depends on the signal kinematics over the full phase space. Specifically, the efficiencies $\epsilon_u$ and $\epsilon_{\rm kin}$ rely on accurate MC simulation, because the particle multiplicities, momenta, and angles depend on the hadronization model for the hadronic states $X_u$.

To simulate the signal $\bar{B} \to X_u \ell \bar{\nu}$ decays we have chosen the prescription by De Fazio and Neubert [39]. Different choices of the parametrization for the Fermi motion of the $b$ quark inside the $B$ meson (Sec. II D) lead to different spectra of the hadron mass $M_X$ and lepton momentum $p^*_\ell$. We estimate the impact of these choices by repeating the analysis with shape function parameters set to values of $\lambda_1^{\rm SF}$ and $\bar{\Lambda}^{\rm SF}$ corresponding to the contour of the $\Delta\chi^2 = 1$ error ellipse [55]. To assess the impact of the choice of the SF ansatz, we repeat this procedure for a different SF ansatz [39].

Since the simulation of $\bar{B} \to X_u \ell \bar{\nu}$ decays is a hybrid of exclusive decays to low-mass charmless mesons and inclusive decays to higher-mass states $X_u$, the relative contributions of the various decays impact the overall kinematics and thereby the efficiencies. We evaluate the impact of varying the branching fractions of the exclusive charmless semileptonic $B$ decays by 1 standard deviation.

The signal losses caused by the kaon veto depend on the production rate of kaons in these decays. In the MC simulation, the number of $K^+$ and $K^0_S$ in the signal decays is set by the probability of producing $s\bar{s}$ quark pairs from the vacuum. The fraction of $s\bar{s}$ events is about 12.0% for the nonresonant component of the signal and is fixed by the parameter $\gamma_s$ in the fragmentation by JETSET [40]. This parameter has been measured by two experiments at center of mass energies between 12 and 36 GeV as $\gamma_s = 0.35 \pm 0.05$ [56], $\gamma_s = 0.27 \pm 0.06$ [57]. We adopt the value $\gamma_s = 0.3$ and estimate the systematic uncertainty by varying the fraction of $s\bar{s}$ events by $\pm 30\%$.

The theoretical uncertainty due to the lower limit on the lepton spectrum is largely accounted for by the reweighting of events for the assessment of the theoretical uncertainty related to the Fermi motion.

### 2. Branching fractions for $B$ and $D$ decays

The exclusive semileptonic branching fractions for $\bar{B} \to X_c \ell \bar{\nu}$ decays and the hadronic mass spectra for these decays are crucial for the determination of the yield of the inclusive normalization sample and the $\bar{B} \to X_c \ell \bar{\nu}$ background. Exclusive $B$ and $D$ branching fractions used in the MC simulation differ slightly from the world averages [34]; this difference is corrected by reweighting events in the simulation. The branching fraction for the sum of semileptonic decays to nonresonant $D^{(*)}\pi$ or broad $D^{**}$ states is taken as the difference between the total semileptonic rate and the other well measured branching fractions, and amounts to about 1.7%.

Similarly, branching fractions and decay distributions for hadronic and semileptonic $D$ meson decays affect the measurement of $\Delta R_{u/sl}$. The effect is different for neutral and charged $B$ mesons, because $\bar{B}^0$ decays mostly into charged $D$ mesons while $B^-$ decays almost always into neutral charm mesons.

Likewise, uncertainties on the form factors for $\bar{B} \to D^{(*)}\ell\bar{\nu}$ decays are taken into account by repeating the analysis with changes of the form factor values by their experimental uncertainties [47]. For $\bar{B} \to D^{**}\ell\bar{\nu}$ decays, the uncertainties on the form factor have not been specified. Thus, we perform the fits with the ISGW2 [58] parametrization of the form factors and take the difference with respect to the default fits as systematic uncertainty.

The uncertainty related to the $\lambda_{D^{**}}$ parameter introduced in Eq. (13) has been estimated by varying it within its uncertainty and taking the difference with respect to the default fits as systematic uncertainty.

#### *3. Combinatorial background subtraction and normalization*

For the fits to the $m_{\rm ES}$ distributions in individual bins of a given kinematic variable, all parameters other than event yields and the ARGUS shape are fixed to values determined from distributions obtained from the full signal sample. To estimate the systematic uncertainty due to this choice of parameters, their values are varied within their statistical uncertainty, taking correlations into account. We estimate the effect of the combinatorial background subtraction by determining it on a simulated sample by means of Monte Carlo truth information and getting the signal yields on data by subtraction. The differences relative to the default fit are taken as systematic uncertainties.

Finally, the uncertainty on the knowledge of the total semileptonic branching fraction adds 1.4% to the assessment of our systematic uncertainty.

In summary, the smallest statistical and systematic uncertainties are achieved for the $M_X < 1.55$ GeV region, which has an acceptance that is reduced by 40% with respect to the region defined by $p^*_\ell > 1.0$ GeV, but has the best separation of signal and background. The dominant systematic uncertainty for samples with no phase space restrictions, except for $p^*_\ell > 1.0$ GeV, is due to the uncertainty on the shape function parameters, which impact the differential $q^2$ and $p^*_\ell$ distributions.

## VI. EXTRACTION OF $|V_{ub}|$

### A. QCD corrections

We extract $|V_{ub}|$ from the measurements of the partial branching fractions $\Delta\mathcal{B}(\bar{B} \to X_u\ell\bar{\nu})$ by relying on QCD predictions. In principle, the total rate for $\bar{B} \to X_u\ell\bar{\nu}$ decays can be calculated based on HQE in powers of $1/m_b$ with uncertainties at the level of 5%, in a similar way as for $\bar{B} \to X_c\ell\bar{\nu}$ decays. Unfortunately, the restrictions imposed on the phase space to reduce the large background from Cabibbo-favored decays spoil the HQE convergence. Perturbative and nonperturbative corrections are drastically enhanced, and the rate becomes sensitive to the Fermi motion of the $b$ quark inside the $B$ meson, introducing terms that are not suppressed by powers of $1/m_b$. In practice, nonperturbative SFs are introduced. The form of the SFs cannot be calculated from first principles. Thus, knowledge of these SFs relies on global fits performed by several collaborations to moments of the lepton energy and hadronic invariant mass in semileptonic $B$ decays, and of the photon energy in radiative $B \to X_s\gamma$ inclusive decays [59–61]. We adopt results of the global fits to published measurements of moments, performed in the kinetic renormalization scheme, specifically the $b$ quark mass $m_b^{\rm kin} = (4.560 \pm 0.023)$ GeV and the mean value of the $b$ quark momentum operator $\mu_\pi^{2(\rm kin)} = (0.453 \pm 0.036)\,\text{GeV}^2$ [46,55]. Because of confinement and nonperturbative effects the quantitative values of the quark mass and other HQE parameters are specific to the theoretical framework in which it is defined. Thus the results of the global fits need to be translated to other schemes, depending on the QCD calculation used to extract $|V_{ub}|$. In the following, we determine $|V_{ub}|$ based on four different QCD calculations. The numerical calculations are based on computer code kindly provided by the authors.

The measured partial branching fractions $\Delta\mathcal{B}(\bar{B} \to X_u\ell\bar{\nu})$ are related to $|V_{ub}|$ via the following equation:

$$|V_{ub}| = \sqrt{\frac{\Delta\mathcal{B}(\bar{B} \to X_u\ell\bar{\nu})}{\tau_B \Delta\Gamma_{\rm theory}}}, \tag{9}$$

where $\Delta\Gamma_{\rm theory}$, the theoretically predicted $\bar{B} \to X_u\ell\bar{\nu}$ rate for the selected phase space region, is based on different QCD calculations, and the $B$ meson lifetime is $\tau_B = 1.582 \pm 0.007$ ps [46]. We adopt the uncertainties on $\Delta\Gamma_{\rm theory}$ as assessed by the authors. It should be noted that the systematic uncertainty on the branching fraction that is related to the uncertainties on the SF parametrization is fully correlated to the theoretical uncertainties discussed here.

The calculated decay rates $\Delta\Gamma_{\rm theory}$ and the resulting $|V_{ub}|$ values are shown for the various kinematic regions in Tables VIII and IX, separately for the four different QCD calculations.

#### *1. BLNP calculation*

The theoretical uncertainties [18–20] arise from the uncertainty on $m_b$, $\mu_\pi^2$, and other nonperturbative corrections, the functional form of the leading and the subleading SFs, the variation of the matching scales, and the uncertainty on the estimated contribution from weak annihilation processes. The dominant contributions are due to the uncertainties on $m_b$ and $\mu_\pi^2$. These parameters need to be translated to the shape function renormalization scheme, for which $m_b^{(\rm SF)} = (4.588 \pm 0.025)$ GeV and $\mu_\pi^{2(\rm SF)} = (0.189 \pm 0.051)\,\text{GeV}^2$. The stated errors include the

TABLE VIII. Results for $|V_{ub}|$ obtained for the four different QCD calculations. The sources of the quoted uncertainties are experimental statistical, experimental systematic, and theory, respectively. The theoretical $\bar{B} \to X \ell \bar{\nu}$ widths, $\Delta\Gamma_{\text{theory}}$ in $\text{ps}^{-1}$, for the various phase space regions examined, as determined from the BLNP, DGE, and GGOU calculations, are also shown. The ADFR calculation uses another methodology (see text); therefore the values for $\Delta\Gamma_{\text{theory}}$ have been obtained by inverting Eq. (9). The $p_\ell^* > 1$ GeV requirement is implicitly assumed in the definitions of phase space regions, unless otherwise noted.

| QCD calculation | Phase space region | $\Delta\Gamma_{\text{theory}}(\text{ps}^{-1})$ | $\lvert V_{ub}\rvert(10^{-3})$ |
|---|---|---|---|
| BLNP | $M_X \leq 1.55$ GeV | $39.3^{+4.7}_{-4.3}$ | $4.17 \pm 0.15 \pm 0.12^{+0.24}_{-0.24}$ |
| | $M_X \leq 1.70$ GeV | $46.1^{+5.0}_{-4.4}$ | $3.97 \pm 0.17 \pm 0.14^{+0.20}_{-0.20}$ |
| | $P_+ \leq 0.66$ GeV | $38.3^{+4.7}_{-4.3}$ | $4.02 \pm 0.18 \pm 0.16^{+0.24}_{-0.23}$ |
| | $M_X \leq 1.70$ GeV, $q^2 \geq 8$ GeV$^2$ | $23.8^{+3.0}_{-2.4}$ | $4.25 \pm 0.19 \pm 0.13^{+0.23}_{-0.25}$ |
| | $M_X - q^2$, $p_\ell^* > 1.0$ GeV | $62.0^{+6.2}_{-5.0}$ | $4.28 \pm 0.15 \pm 0.18^{+0.18}_{-0.20}$ |
| | $p_\ell^* > 1.0$ GeV | $62.0^{+6.2}_{-5.0}$ | $4.30 \pm 0.18 \pm 0.21^{+0.18}_{-0.20}$ |
| | $p_\ell^* > 1.3$ GeV | $52.8^{+5.3}_{-4.3}$ | $4.29 \pm 0.18 \pm 0.20^{+0.19}_{-0.20}$ |
| DGE | $M_X \leq 1.55$ GeV | $35.3^{+3.3}_{-3.5}$ | $4.40 \pm 0.16 \pm 0.12^{+0.24}_{-0.19}$ |
| | $M_X \leq 1.70$ GeV | $42.0^{+4.8}_{-4.8}$ | $4.16 \pm 0.18 \pm 0.14^{+0.26}_{-0.22}$ |
| | $P_+ \leq 0.66$ GeV | $36.9^{+5.5}_{-5.8}$ | $4.10 \pm 0.19 \pm 0.17^{+0.37}_{-0.28}$ |
| | $M_X \leq 1.70$ GeV, $q^2 \geq 8$ GeV$^2$ | $24.4^{+2.4}_{-2.0}$ | $4.19 \pm 0.19 \pm 0.12^{+0.18}_{-0.19}$ |
| | $M_X - q^2$, $p_\ell^* > 1.0$ GeV | $58.7^{+3.5}_{-3.2}$ | $4.40 \pm 0.16 \pm 0.18^{+0.12}_{-0.13}$ |
| | $p_\ell^* > 1.0$ GeV | $58.7^{+3.5}_{-3.2}$ | $4.42 \pm 0.19 \pm 0.23^{+0.13}_{-0.13}$ |
| | $p_\ell^* > 1.3$ GeV | $50.4^{+3.3}_{-3.0}$ | $4.39 \pm 0.19 \pm 0.20^{+0.15}_{-0.14}$ |
| GGOU | $M_X \leq 1.55$ GeV | $41.0^{+4.6}_{-3.8}$ | $4.08 \pm 0.15 \pm 0.11^{+0.20}_{-0.21}$ |
| | $M_X \leq 1.70$ GeV | $46.8^{+4.2}_{-3.6}$ | $3.94 \pm 0.17 \pm 0.14^{+0.16}_{-0.17}$ |
| | $P_+ \leq 0.66$ GeV | $44.0^{+8.6}_{-6.3}$ | $3.75 \pm 0.17 \pm 0.15^{+0.30}_{-0.32}$ |
| | $M_X \leq 1.70$ GeV, $q^2 \geq 8$ GeV$^2$ | $24.7^{+3.2}_{-2.4}$ | $4.17 \pm 0.18 \pm 0.12^{+0.22}_{-0.25}$ |
| | $M_X - q^2$, $p_\ell^* > 1.0$ GeV | $60.2^{+3.0}_{-2.5}$ | $4.35 \pm 0.16 \pm 0.18^{+0.09}_{-0.10}$ |
| | $p_\ell^* > 1.0$ GeV | $60.2^{+3.0}_{-2.5}$ | $4.36 \pm 0.19 \pm 0.23^{+0.09}_{-0.10}$ |
| | $p_\ell^* > 1.3$ GeV | $51.8^{+2.8}_{-2.3}$ | $4.33 \pm 0.18 \pm 0.20^{+0.10}_{-0.11}$ |
| ADFR | $M_X \leq 1.55$ GeV | $47.1^{+5.2}_{-4.3}$ | $3.81 \pm 0.14 \pm 0.11^{+0.18}_{-0.20}$ |
| | $M_X \leq 1.70$ GeV | $52.3^{+5.4}_{-4.5}$ | $3.73 \pm 0.16 \pm 0.13^{+0.17}_{-0.18}$ |
| | $P_+ \leq 0.66$ GeV | $48.9^{+5.6}_{-4.6}$ | $3.56 \pm 0.16 \pm 0.15^{+0.18}_{-0.19}$ |
| | $M_X \leq 1.70$ GeV, $q^2 \geq 8$ GeV$^2$ | $30.9^{+3.0}_{-2.5}$ | $3.74 \pm 0.16 \pm 0.11^{+0.16}_{-0.17}$ |
| | $M_X - q^2$, $p_\ell^* > 1.0$ GeV | $62.0^{+5.7}_{-5.0}$ | $4.29 \pm 0.15 \pm 0.18^{+0.18}_{-0.19}$ |
| | $p_\ell^* > 1.0$ GeV | $62.0^{+5.7}_{-5.0}$ | $4.30 \pm 0.19 \pm 0.23^{+0.18}_{-0.19}$ |
| | $p_\ell^* > 1.3$ GeV | $53.3^{+5.1}_{-4.4}$ | $4.27 \pm 0.18 \pm 0.19^{+0.18}_{-0.19}$ |

uncertainties due to higher order terms that are neglected in the translation from one scheme to another.

A recent calculation at next-to-next-to-leading order (NNLO) [62] indicates that the differences with respect to NLO calculations are rather large. They would increase the value of $|V_{ub}|$ by about 8%, suggesting that the current uncertainties are underestimated. Similar effects might also be present for other QCD calculations, but estimates are not yet available.

#### *2. DGE calculation*

The theoretical uncertainties [21,22] arise from the uncertainty on $\alpha_s$, the uncertainty on $m_b$, and other nonperturbative corrections, for instance, the variation of the matching scales and the uncertainty on the weak annihilation. The dominant error is the uncertainty on $m_b$ for which the $\overline{\text{MS}}$ renormalization scheme is used. Therefore the results of the global fit had to be translated to the $\overline{\text{MS}}$

TABLE IX. Summary of the fitted number of events $N_u$, the efficiencies, the partial branching fractions $\Delta\mathcal{B}(\bar{B} \to X_u \ell \bar{\nu})$ and $|V_{ub}|(10^{-3})$ based on four different QCD calculations of the hadronic matrix element as a function of the lower limit on the lepton momentum $p^*_\ell$. The uncertainties on $\Delta\mathcal{B}(\bar{B} \to X_u \ell \bar{\nu})$ are statistical and systematic, and those for $|V_{ub}|$ are statistical, systematic, and theoretical. The uncertainties on all other parameters are statistical. $|V_{ub}|$ values for BLNP and GGOU are not provided above 2.2 GeV due to large uncertainties.

| $p^*_{\ell_{\min}}$(GeV) | $N_u$ | $\epsilon^u_{\rm sel}\epsilon^u_{\rm kin}$ | $\frac{\epsilon^{\rm sl}_\ell \epsilon^{\rm sl}_{\rm tag}}{\epsilon^u_\ell \epsilon^u_{\rm tag}}$ | $\Delta\mathcal{B}(\bar{B} \to X_u \ell \bar{\nu})(10^{-3})$ | $\lvert V_{ub}\rvert$BLNP$(10^{-3})$ | $\lvert V_{ub}\rvert$GGOU$(10^{-3})$ | $\lvert V_{ub}\rvert$DGE$(10^{-3})$ | $\lvert V_{ub}\rvert$ADFR$(10^{-3})$ |
|---|---|---|---|---|---|---|---|---|
| **1.0** | $1470 \pm 130$ | $0.342 \pm 0.002$ | $1.18 \pm 0.03$ | $1.81 \pm 0.16 \pm 0.19$ | $4.30 \pm 0.18 \pm 0.21^{+0.18}_{-0.20}$ | $4.36 \pm 0.19 \pm 0.23^{+0.09}_{-0.10}$ | $4.42 \pm 0.19 \pm 0.23^{+0.13}_{-0.13}$ | $4.30 \pm 0.19 \pm 0.23^{+0.18}_{-0.19}$ |
| **1.1** | $1440 \pm 127$ | $0.345 \pm 0.002$ | $1.18 \pm 0.19$ | $1.75 \pm 0.15 \pm 0.18$ | $4.32 \pm 0.17 \pm 0.19^{+0.18}_{-0.20}$ | $4.38 \pm 0.19 \pm 0.22^{+0.09}_{-0.11}$ | $4.44 \pm 0.19 \pm 0.23^{+0.14}_{-0.13}$ | $4.34 \pm 0.19 \pm 0.22^{+0.20}_{-0.20}$ |
| **1.2** | $1421 \pm 124$ | $0.353 \pm 0.002$ | $1.18 \pm 0.05$ | $1.69 \pm 0.14 \pm 0.18$ | $4.36 \pm 0.17 \pm 0.22^{+0.19}_{-0.21}$ | $4.41 \pm 0.18 \pm 0.23^{+0.10}_{-0.11}$ | $4.47 \pm 0.19 \pm 0.24^{+0.14}_{-0.14}$ | $4.36 \pm 0.18 \pm 0.23^{+0.20}_{-0.20}$ |
| **1.3** | $1329 \pm 121$ | $0.363 \pm 0.002$ | $1.18 \pm 0.09$ | $1.53 \pm 0.13 \pm 0.14$ | $4.29 \pm 0.18 \pm 0.20^{+0.19}_{-0.20}$ | $4.33 \pm 0.18 \pm 0.20^{+0.10}_{-0.11}$ | $4.39 \pm 0.19 \pm 0.20^{+0.15}_{-0.14}$ | $4.27 \pm 0.18 \pm 0.19^{+0.18}_{-0.19}$ |
| **1.4** | $1381 \pm 114$ | $0.368 \pm 0.002$ | $1.18 \pm 0.04$ | $1.58 \pm 0.13 \pm 0.14$ | $4.52 \pm 0.17 \pm 0.18^{+0.20}_{-0.22}$ | $4.55 \pm 0.19 \pm 0.20^{+0.11}_{-0.12}$ | $4.61 \pm 0.19 \pm 0.20^{+0.16}_{-0.15}$ | $4.48 \pm 0.18 \pm 0.20^{+0.21}_{-0.21}$ |
| **1.5** | $1383 \pm 107$ | $0.378 \pm 0.003$ | $1.19 \pm 0.02$ | $1.53 \pm 0.12 \pm 0.14$ | $4.66 \pm 0.16 \pm 0.18^{+0.21}_{-0.23}$ | $4.67 \pm 0.18 \pm 0.21^{+0.11}_{-0.14}$ | $4.74 \pm 0.19 \pm 0.22^{+0.17}_{-0.17}$ | $4.59 \pm 0.18 \pm 0.21^{+0.21}_{-0.22}$ |
| **1.6** | $1248 \pm 99$ | $0.390 \pm 0.003$ | $1.17 \pm 0.03$ | $1.35 \pm 0.10 \pm 0.13$ | $4.64 \pm 0.17 \pm 0.20^{+0.21}_{-0.23}$ | $4.63 \pm 0.17 \pm 0.22^{+0.12}_{-0.15}$ | $4.69 \pm 0.17 \pm 0.23^{+0.18}_{-0.18}$ | $4.52 \pm 0.17 \pm 0.22^{+0.21}_{-0.21}$ |
| **1.7** | $1158 \pm 90$ | $0.404 \pm 0.003$ | $1.16 \pm 0.03$ | $1.22 \pm 0.09 \pm 0.12$ | $4.71 \pm 0.17 \pm 0.20^{+0.22}_{-0.24}$ | $4.68 \pm 0.17 \pm 0.23^{+0.14}_{-0.16}$ | $4.73 \pm 0.17 \pm 0.23^{+0.21}_{-0.19}$ | $4.53 \pm 0.17 \pm 0.22^{+0.21}_{-0.22}$ |
| **1.8** | $1043 \pm 80$ | $0.418 \pm 0.003$ | $1.16 \pm 0.04$ | $1.07 \pm 0.08 \pm 0.10$ | $4.79 \pm 0.17 \pm 0.21^{+0.23}_{-0.25}$ | $4.71 \pm 0.18 \pm 0.22^{+0.15}_{-0.18}$ | $4.75 \pm 0.18 \pm 0.22^{+0.23}_{-0.20}$ | $4.51 \pm 0.17 \pm 0.21^{+0.21}_{-0.22}$ |
| **1.9** | $845 \pm 69$ | $0.430 \pm 0.004$ | $1.14 \pm 0.06$ | $0.85 \pm 0.07 \pm 0.10$ | $4.76 \pm 0.18 \pm 0.23^{+0.23}_{-0.26}$ | $4.63 \pm 0.19 \pm 0.27^{+0.17}_{-0.21}$ | $4.64 \pm 0.19 \pm 0.27^{+0.26}_{-0.22}$ | $4.36 \pm 0.18 \pm 0.26^{+0.20}_{-0.21}$ |
| **2.0** | $567 \pm 56$ | $0.457 \pm 0.004$ | $1.11 \pm 0.04$ | $0.55 \pm 0.05 \pm 0.06$ | $4.41 \pm 0.20 \pm 0.20^{+0.24}_{-0.28}$ | $4.22 \pm 0.19 \pm 0.23^{+0.18}_{-0.23}$ | $4.19 \pm 0.19 \pm 0.23^{+0.27}_{-0.23}$ | $3.86 \pm 0.18 \pm 0.21^{+0.19}_{-0.20}$ |
| **2.1** | $432 \pm 44$ | $0.474 \pm 0.005$ | $1.07 \pm 0.03$ | $0.42 \pm 0.04 \pm 0.05$ | $4.68 \pm 0.22 \pm 0.24^{+0.31}_{-0.37}$ | $4.37 \pm 0.21 \pm 0.26^{+0.24}_{-0.32}$ | $4.25 \pm 0.20 \pm 0.25^{+0.35}_{-0.29}$ | $3.82 \pm 0.18 \pm 0.23^{+0.18}_{-0.19}$ |
| **2.2** | $339 \pm 29$ | $0.499 \pm 0.007$ | $1.02 \pm 0.04$ | $0.33 \pm 0.03 \pm 0.03$ | $5.51 \pm 0.22 \pm 0.23^{+0.57}_{-0.68}$ | $5.02 \pm 0.23 \pm 0.23^{+0.48}_{-0.61}$ | $4.62 \pm 0.21 \pm 0.21^{+0.50}_{-0.43}$ | $4.00 \pm 0.18 \pm 0.18^{+0.19}_{-0.21}$ |
| **2.3** | $227 \pm 19$ | $0.521 \pm 0.009$ | $1.00 \pm 0.04$ | $0.22 \pm 0.02 \pm 0.02$ | — | — | $5.15 \pm 0.24 \pm 0.24^{+0.92}_{-0.79}$ | $4.17 \pm 0.19 \pm 0.19^{+0.22}_{-0.25}$ |
| **2.4** | $82 \pm 9$ | $0.539 \pm 0.013$ | $1.00 \pm 0.08$ | $0.08 \pm 0.01 \pm 0.01$ | — | — | $5.11 \pm 0.34 \pm 0.34^{+2.08}_{-1.92}$ | $3.67 \pm 0.24 \pm 0.24^{+0.23}_{-0.26}$ |

scheme, $m_b^{\overline{\rm MS}} = (4.194 \pm 0.043)$ GeV, where the uncertainty includes the uncertainty on the translation.

#### 3. GGOU calculation

The theoretical uncertainties [25] in the determinations of the widths and $|V_{ub}|$ from the GGOU calculations arise from the uncertainty on $\alpha_s$, $m_b$, and $\mu_\pi^2$, plus various nonperturbative corrections: the modeling of the $q^2$ tail and choice of the scale $q_*^2$, the functional form of the distribution functions, and the uncertainty on the weak annihilation rate. The dominant error originates from the uncertainties on $m_b$ and $\mu_\pi^2$. Since GGOU calculations are based on the kinetic renormalization scheme, there is no need for translation.

#### 4. ADFR calculation

The ADFR calculation [23,24] relates $\Delta\mathcal{B}(\bar{B} \to X_u \ell \bar{\nu})$ to $|V_{ub}|$ in a way that is different from the other three calculations discussed above. In the framework of ADFR, the partial branching ratio is expressed in terms of $R_{c/u}$,

$$\Delta\mathcal{B}(\bar{B} \to X_u \ell \bar{\nu}) = \frac{\mathcal{B}(\bar{B} \to X \ell \bar{\nu})}{1 + R_{c/u}} W, \tag{10}$$

where $W = \Delta\Gamma(\bar{B} \to X_u \ell \bar{\nu})/\Gamma(\bar{B} \to X_u \ell \bar{\nu})$ is the fraction of the charmless branching fraction in a selected kinematic region and $\mathcal{B}(\bar{B} \to X \ell \bar{\nu})$ is the total semileptonic branching fraction. $R_{c/u}$ is related to $|V_{ub}|$ as

$$R_{c/u} = \frac{|V_{cb}|^2}{|V_{ub}|^2} I(\rho) G(\alpha_s, \rho). \tag{11}$$

The function $I(\rho)$ accounts for the suppression of phase space due to $m_c$ and $I(\rho) = 1 - 8\rho + 12\rho^2 \log(1/\rho) + 8\rho^2 - \rho^4$, with $\rho \equiv m_c^2/m_b^2 \approx 0.1$. The factor $G(\alpha_s, \rho)$ contains corrections suppressed by powers of $\alpha_s$ and powers of $\rho$,

$$G(\alpha_s, \rho) = 1 + \sum_{n=1}^{\infty} G_n(\rho) \alpha_s^n, \tag{12}$$

with $G_n(0) = 0$. The errors of the ADFR calculations arise from the uncertainty in $\alpha_s$, $|V_{cb}|$, the quark masses $m_b$ and $m_c$, and the uncertainty on $\mathcal{B}(\bar{B} \to X \ell \bar{\nu})$. The dominant uncertainty is due to the uncertainty on the mass $m_c$.

### B. $|V_{ub}|$ extraction

We present the results for $|V_{ub}|$ with statistical, systematic, and theoretical uncertainties in Table VIII. Values of $|V_{ub}|$ extracted from partial branching fractions for samples with the lower limit on the lepton momentum $p_\ell^*$ varying from 1.0 GeV to 2.4 GeV are tabulated in Table IX. The different values of $|V_{ub}|$ are consistent within 1 standard deviation and equally consistent with the previous *BABAR* measurements of $|V_{ub}|$ on inclusive charmless semileptonic $B$ decays [11,15,16] as well as a similar measurement by the Belle Collaboration [17].

Our result on the study of the lepton spectrum above 2 GeV can be compared to what *BABAR* [15,16], Belle [14], and CLEO [13] have published on the analysis of the lepton end-point spectrum in untagged $B$ decays. Experimental uncertainties are comparable, as well as theoretical uncertainties, which are quite large in this region of phase space. The values of $|V_{ub}|$ obtained with such different techniques agree very well.

We have evaluated the correlations of the measurements of $|V_{ub}|$ in selected regions of phase space taking into account the experimental and theoretical procedures, as presented in Table IV. The theoretical correlations have been obtained for the BLNP calculations by taking several values of the heavy quark parameters within their uncertainties and computing the correlation of the acceptance for pairs of phase space regions. The resulting correlation coefficients are in all cases greater than 97%. It is assumed that the correlations are also close to 100% for the other three theory calculations.

We choose to quote the $|V_{ub}|$ value corresponding to the most inclusive measurement, namely, the one based on the two-dimensional fit of the $M_X - q^2$ distribution with no phase space restrictions, except for $p_\ell^* > 1.0$ GeV. We calculate the arithmetic average of the values and uncertainties obtained with the different theoretical calculations shown above and find

$$|V_{ub}| = (4.33 \pm 0.24 \pm 0.15) \times 10^{-3}, \tag{13}$$

where the first uncertainty is experimental and the second theoretical.

A calculation specifically suited for phase space regions defined by the $M_X$ and $q^2$ cuts [63] can also be considered. This uses as input the $b$ quark mass in the $1S$ scheme [64], $m_b^{1S} = 4.704 \pm 0.029$ GeV, determined by a global fit in that scheme, similar to the one described in Sec. VI A. The resulting value of $|V_{ub}|$ for the phase space region defined by $M_X < 1.7$ GeV, $q^2 > 8$ GeV$^2$ is $|V_{ub}| = (4.50 \pm 0.24 \pm 0.29) \times 10^{-3}$, slightly larger but still in agreement with the other theoretical calculations.

### C. Limits on weak annihilation

The measurements of $\Delta\mathcal{B}(\bar{B} \to X_u \ell \bar{\nu})$, separately for neutral and charged $B$ mesons, are summarized in Table V for the various kinematic selections. These results are used to test isospin invariance, based on the ratio

$$R = \frac{\Delta\Gamma^-}{\Delta\Gamma^0} = \frac{\tau^0}{\tau^-} \frac{\Delta\mathcal{B}(B^- \to X_u \ell \nu)}{\Delta\mathcal{B}(\bar{B}^0 \to X_u \ell \nu)}, \tag{14}$$

where $\tau^-/\tau^0 = 1.071 \pm 0.009$ [34] is the ratio of the lifetimes for $B^-$ and $\bar{B}^0$. For the $M_X < 1.55$ GeV selection, we

obtain $R - 1 = 0.03 \pm 0.15 \pm 0.18$, where the first uncertainty is statistical and the second is systematic. This result is consistent with zero; similar results, with larger uncertainties, are obtained for the other regions of phase space listed in Table V. Thus, we have no evidence for a difference between partial decay rates for $B^-$ and $\bar{B}^0$. If we define the possible contribution of the weak annihilation as $\Delta\Gamma_{WA} = \Delta\Gamma^- - \Delta\Gamma^0$, its relative contribution to the partial decay width $\Delta\Gamma$ for $\bar{B} \to X_u \ell \bar{\nu}$ decays is $\Delta\Gamma_{WA}/\Delta\Gamma = R - 1$. With $f_{WA}$ defined as the fraction of weak annihilation contribution for a specific kinematic region and $f_u$ defined as the fraction of $\bar{B} \to X_u \ell \bar{\nu}$ events predicted for that region, we can write $\Delta\Gamma_{WA} = f_{WA}\Gamma_{WA}$ and $\Delta\Gamma = f_u\Gamma$, where $\Gamma$ is the total decay width of $\bar{B} \to X_u \ell \bar{\nu}$ decays. Thus the relative contribution of the weak annihilation is

$$\frac{\Gamma_{WA}}{\Gamma} = \frac{f_u}{f_{WA}}(R - 1). \tag{15}$$

Since the weak annihilation is expected to be confined to the high $q^2$ region, it is reasonable to assume $f_{WA} = 1.0$ for all the kinematic selections. We adopt the prediction for $f_u$ by De Fazio–Neubert (see Sec. II D) and place limits on $\Gamma_{WA}/\Gamma$. The most stringent limit is obtained for the selection $M_X < 1.55$ GeV, namely, $-0.17 \leq (\Gamma_{WA}/\Gamma) < 0.19$ at 90% confidence level (C.L.). This model-independent limit on WA is consistent, but weaker than the limit derived by the CLEO Collaboration [65] on the basis of an assumed $q^2$ distribution. Both limits are larger than the theoretical limits, estimated from $D$ and $D_s$ semileptonic decay rates, of 3% [26,27], and the more recent and stringent one of less than 2% [28,29].

## VII. CONCLUSIONS

In summary, we have measured the branching fractions for inclusive charmless semileptonic $B$ decays $\bar{B} \to X_u \ell \bar{\nu}$, in various overlapping regions of phase space, based on the full *BABAR* data sample. The results are presented for the full sample, and also separately for charged and neutral $B$ mesons.

We have extracted the magnitude of the CKM element $|V_{ub}|$ based on several theoretical calculations. Measurements in different phase space regions are consistent for all sets of calculations, within their uncertainties. Correlations between $|V_{ub}|$ measurements, including both experimental and theoretical uncertainties are presented. They are close to 100% for the theoretical input.

We have obtained the most precise results from the analysis based on the two-dimensional fit to $M_X - q^2$, with no restriction other than $p_\ell^* > 1.0$ GeV. The total uncertainty is about 7%, comparable in precision to the result recently presented by the Belle Collaboration [17] which uses a multivariate discriminant to reduce the combinatorial background. The results presented here supersede earlier *BABAR* measurements based on a smaller tagged sample of events [11].

We have found no evidence for isospin violation; the difference between the partial branching fractions for $\bar{B}^0$ and $B^-$ is consistent with zero. Based on this measurement, we place a limit on a potential contribution from weak annihilation of 19% of the total charmless semileptonic branching faction at 90% C.L., which is still larger than recent theoretical expectations [28,29].

Improvements in these measurements will require larger tagged data samples recorded with improved detectors and much improved understanding of the simulation of semileptonic $B$ decays, both background decays involving charm mesons as well as exclusive and inclusive decays contributing to the signal. Reductions in the theoretical uncertainties are expected to come from improved QCD calculations for $\bar{b} \to u \ell \bar{\nu}$ and $b \to s\gamma$ transitions, combined with improved information on the $b$ quark mass and measurements of radiative $B$ decays.

## ACKNOWLEDGMENTS

We thank Matthias Neubert, Gil Paz, Einan Gardi, Paolo Gambino, Paolo Giordano, Ugo Aglietti, Giancarlo Ferrera, and Giulia Ricciardi for useful discussions and for providing the software tools and code that enabled us to compute $|V_{ub}|$ values from measured branching fractions. We are grateful for the extraordinary contributions of our PEP-II colleagues in achieving the excellent luminosity and machine conditions that have made this work possible. The success of this project also relies critically on the expertise and dedication of the computing organizations that support *BABAR*. The collaborating institutions wish to thank SLAC for its support and the kind hospitality extended to them. This work is supported by the U.S. Department of Energy and National Science Foundation, the Natural Sciences and Engineering Research Council (Canada), the Commissariat à l'Energie Atomique and Institut National de Physique Nucléaire et de Physique des Particules (France), the Bundesministerium für Bildung und Forschung and Deutsche Forschungsgemeinschaft (Germany), the Istituto Nazionale di Fisica Nucleare (Italy), the Foundation for Fundamental Research on Matter (The Netherlands), the Research Council of Norway, the Ministry of Education and Science of the Russian Federation, Ministerio de Ciencia e Innovación (Spain), and the Science and Technology Facilities Council (United Kingdom). Individuals have received support from the Marie-Curie IEF program (European Union), the A. P. Sloan Foundation (USA), and the Binational Science Foundation (USA-Israel).

[1] N. Cabibbo, Phys. Rev. Lett. **10**, 531 (1963).
[2] M. Kobayashi and T. Maskawa, Prog. Theor. Phys. **49**, 652 (1973).
[3] J. D. Bjorken, SLAC Report No. 378, p. 167, 1990.
[4] R. Kowalewski and T. Mannel, J. Phys. G **37**, 075021 (2010).
[5] M. Antonelli *et al.*, Phys. Rep. **494**, 197 (2010).
[6] A. Bevan *et al.* (UTfit Collaboration), Proc. Sci., ICHEP2010 (2010) 270.
[7] J. Charles, A. Hocker, H. Lacker, S. Laplace, F. R. Le Diberder, J. Malcles, J. Ocariz, M. Pivk, and L. Roos (CKMfitter Collaboration), Eur. Phys. J. C **41**, 1 (2005).
[8] A. V. Manohar and M. B. Wise, Phys. Rev. D **49**, 1310 (1994).
[9] I. I. Y. Bigi, B. Blok, M. A. Shifman, and A. I. Vainshtein, Phys. Lett. B **323**, 408 (1994).
[10] Charge-conjugate modes are implied throughout this paper, unless explicitly stated.
[11] B. Aubert *et al.* (*BABAR* Collaboration), Phys. Rev. Lett. **100**, 171802 (2008).
[12] J. E. Bartelt *et al.* (CLEO Collaboration), Phys. Rev. Lett. **71**, 4111 (1993).
[13] A. Bornheim *et al.* (CLEO Collaboration), Phys. Rev. Lett. **88**, 231803 (2002).
[14] A. Limosani *et al.* (Belle Collaboration), Phys. Lett. B **621**, 28 (2005).
[15] B. Aubert *et al.* (*BABAR* Collaboration), Phys. Rev. D **73**, 012006 (2006).
[16] B. Aubert *et al.* (*BABAR* Collaboration), Phys. Rev. Lett. **95**, 111801 (2005).**97**, 019903(E) (2006).
[17] P. Urquijo *et al.* (Belle Collaboration), Phys. Rev. Lett. **104**, 021801 (2010).
[18] B. O. Lange, M. Neubert, and G. Paz, Phys. Rev. D **72**, 073006 (2005).
[19] S. W. Bosch, B. O. Lange, M. Neubert, and G. Paz, Nucl. Phys. **B699**, 335 (2004).
[20] S. W. Bosch, M. Neubert, and G. Paz, J. High Energy Phys. 11 (2004), 073.
[21] J. R. Andersen and E. Gardi, J. High Energy Phys. 01 (2006) 097.
[22] E. Gardi, arXiv:0806.4524.
[23] U. Aglietti, F. Di Lodovico, G. Ferrera, and G. Ricciardi, Eur. Phys. J. C **59**, 831 (2009).
[24] U. Aglietti, G. Ferrera, and G. Ricciardi, Nucl. Phys. **B768**, 85 (2007), and references therein.
[25] P. Gambino, P. Giordano, G. Ossola, and N. Uraltsev, J. High Energy Phys. 10 (2007) 058.
[26] I. I. Bigi and N. Uraltsev, Nucl. Phys. **B423**, 33 (1994).
[27] M. B. Voloshin, Phys. Lett. B **515**, 74 (2001).
[28] Z. Ligeti, M. Luke, and A. V. Manohar, Phys. Rev. D **82**, 033003 (2010).
[29] P. Gambino and J. F. Kamenik, Nucl. Phys. **B840**, 424 (2010).
[30] B. Aubert *et al.* (*BABAR* Collaboration), Nucl. Instrum. Methods Phys. Res., Sect. A **479**, 1 (2002).
[31] B. Aubert *et al.* (BABAR Collaboration), Phys. Rev. D **66**, 032003 (2002).
[32] S. Agostinelli *et al.* (GEANT4 Collaboration), Nucl. Instrum. Methods Phys. Res., Sect. A **506**, 250 (2003).
[33] D. J. Lange, Nucl. Instrum. Methods Phys. Res., Sect. A **462**, 152 (2001).
[34] K. Nakamura *et al.* (Particle Data Group), J. Phys. G **37**, 075021 (2010).
[35] D. Becirevic and A. B. Kaidalov, Phys. Lett. B **478**, 417 (2000).
[36] B. Aubert *et al.* (*BABAR* Collaboration), Phys. Rev. Lett. **98**, 091801 (2007).
[37] P. Ball and R. Zwicky, Phys. Rev. D **71**, 014015 (2005).
[38] P. Ball and R. Zwicky, Phys. Rev. D **71**, 014029 (2005).
[39] F. De Fazio and M. Neubert, J. High Energy Phys. 06 (1999) 017.
[40] T. Sjœstrand, Comput. Phys. Commun. **82**, 74 (1994).
[41] I. Caprini, L. Lellouch, and M. Neubert, Nucl. Phys. **B530**, 153 (1998).
[42] B. Grinstein, Nucl. Phys. **B339**, 253 (1990).
[43] E. Eichten and B. R. Hill, Phys. Lett. B **234**, 511 (1990).
[44] H. Georgi, Phys. Lett. B **240**, 447 (1990).
[45] A. F. Falk, H. Georgi, B. Grinstein, and M. B. Wise, Nucl. Phys. **B343**, 1 (1990).
[46] Y. Amhis *et al.* (Heavy Flavour Averaging Group), arXiv:1207.1158.
[47] B. Aubert *et al.* (*BABAR* Collaboration), Phys. Rev. D **79**, 012002 (2009).
[48] B. Aubert *et al.* (*BABAR* Collaboration), Phys. Rev. Lett. **104**, 011802 (2010).
[49] B. Aubert *et al.* (*BABAR* Collaboration), Phys. Rev. D **77**, 032002 (2008).
[50] A. K. Leibovich, Z. Ligeti, I. W. Stewart, and M. B. Wise, Phys. Rev. D **57**, 308 (1998).
[51] J. L. Goity and W. Roberts, Phys. Rev. D **51**, 3459 (1995).
[52] H. Albrecht *et al.* (ARGUS Collaboration), Z. Phys. C **48**, 543 (1990).
[53] T. Skwarnicki *et al.* (Crystal Ball Collaboration), DESY Internal Report No. F31-86-02, 1986.
[54] B. Aubert *et al.* (*BABAR* Collaboration), Phys. Rev. D **74**, 091105 (2006).
[55] C. Schwanda *et al.* (Belle Collaboration), Phys. Rev. D **78**, 032016 (2008).
[56] M. Althoff *et al.* (TASSO Collaboration), Z. Phys. C **27**, 27 (1985).
[57] W. Bartel *et al.* (JADE Collaboration), Z. Phys. C **20**, 187 (1983).
[58] N. Isgur and D. Scora, Phys. Rev. D **52**, 2783 (1995).
[59] P. Gambino and N. Uraltsev, Eur. Phys. J. C **34**, 181 (2004).
[60] C. W. Bauer, Z. Ligeti, M. Luke, A. V. Manohar, and M. Trott, Phys. Rev. D **70**, 094017 (2004).
[61] D. Benson, I. I. Bigi, and N. Uraltsev, Nucl. Phys. **B710**, 371 (2005).
[62] C. Greub, M. Neubert, and B. D. Pecjak, Eur. Phys. J. C **65**, 501 (2010).
[63] C. W. Bauer, Z. Ligeti, and M. Luke, Phys. Rev. D **64**, 113004 (2001).
[64] C. W. Bauer, Z. Ligeti, M. Luke, and A. V. Manohar, Phys. Rev. D **67**, 054012 (2003); **70**, 094017 (2004).
[65] J. L. Rosner *et al.* (JADE Collaboration), Phys. Rev. Lett. **96**, 121801 (2006).